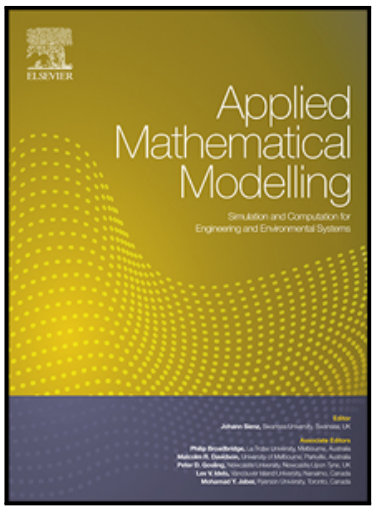

Vibration Analysis for Anti-Symmetric Laminated Composite Plates Resting on Visco-Elastic Foundation with Temperature Effects

A. Rahmani , S. Faroughi , M.I. Friswell

PII: S0307-904X(21)00035-4
DOI: https://doi.org/10.1016/j.apm.2021.01.026
Reference: APM 13876

To appear in: *Applied Mathematical Modelling*

Received date: 10 June 2020
Revised date: 19 December 2020
Accepted date: 14 January 2021

Please cite this article as: A. Rahmani , S. Faroughi , M.I. Friswell , Vibration Analysis for Anti-Symmetric Laminated Composite Plates Resting on Visco-Elastic Foundation with Temperature Effects, *Applied Mathematical Modelling* (2021), doi: https://doi.org/10.1016/j.apm.2021.01.026

Highlights

Vibration Analysis for Anti-Symmetric Laminated Composite Plates Resting on Visco-Elastic Foundations with Temperature Effects

A. Rahmani, S. Faroughi, M.I. Friswell

1- *Comprehensive vibrational analysis of anti-symmetric laminated composite plates.*
2- *Vibrational analysis includes an elastic foundation and thermal effects.*
3- *HSDT is applied to estimate the effects of the higher-order transverse shear.*
4- *Effects of damping, elastic, aspect and slenderness ratios are discussed in detail.*
5- *Different anti-symmetric laminates and boundary conditions are considered.*

Vibration Analysis for Anti-Symmetric Laminated Composite Plates Resting on Visco-Elastic Foundation with Temperature Effects

A. Rahmani[1], S. Faroughi[1], M.I. Friswell[2] [1*]

[1]Faculty of Mechanical Engineering, Urmia University of Technology, Urmia, Iran
[2]College of Engineering, Swansea University, Swansea, UK

Abstract

In this work, a comprehensive vibrational behavior analysis is performed on anti-symmetric laminated composite plates resting on visco-elastic foundations undergoing thermal effects. Here, *the governing equations of motion are developed through Hamilton's principle* and *Reddy's plate* theory as higher-order shear deformation theory (HSDT) is employed to capture high accuracy. Also, the generalized differential quadrature method (GDQM) is used to predict the vibration response and the natural frequencies. The effects of temperature change, Winkler-Pasternak and damping coefficients for the elastic foundation, the elastic ratio, the arrangement of different anti-symmetric laminates, and the aspect and slenderness ratios are observed and discussed in detail. The results are extracted for fully clamped boundary conditions and the effects of other boundary conditions are also illustrated.

Keywords: Anti-symmetric Laminated Composite Plates; Thermal Effects; Elastic Foundation; Higher-Order Shear Deformation Theory; GDQM

1. Introduction

In recent years, the applications of composite structures such as laminated composite plates and shells have increased progressively in almost all industries such as aeronautical, aerospace and satellites, marine, civil and large space structures, automotive, sports goods, and medical devices, because of their outstanding mechanical properties such as high stiffness to weight, high strength to weight and low maintenance cost. For example, more than 50% of aeronautical structures in the A350 XWB and Boeing 787 aircraft are composite. Meanwhile, anisotropic and symmetric/asymmetric/anti-symmetric laminated composite plates have been extensively used in weight sensitive engineering structures from aerospace applications to infrastructures and car industries [1-4]. Accordingly, to achieve a proper design and to increase the safety and reliability,

Corresponding author: m.i.friswell@swansea.ac.uk [1*]

the accurate evaluation and detailed study of mechanical behaviors, such as bending, buckling, vibration and wave propagation of plates, is required. Hence, many researchers have considered a range of static and dynamic analysis of laminated composite structures, especially symmetric/asymmetric/anti-symmetric laminated composite plates recently [5-11]. Therefore, the following brief literature review considers recent papers that investigate the mechanical behavior of laminated composite structures.

There are many approaches to analyze laminated composite plates, such as classical, first and higher order shear deformation theories and also layer-wise theory, which have attracted the interest of many researchers [12-15]. Classical (CLT) and first order shear deformation (FSDT) theories have been extensively employed for the vibration analysis of anisotropic laminated composite plates and shells [16-20]. Nevertheless, higher-order shear deformation theory and layer-wise theories have given accurate results especially for thick laminated composite plates [21].

Thai and Kim [22] analyzed the free vibration of laminated composite plates. They derived the equations of motion through two variable refined plate theory and Hamilton's principle. They employed Navier*'s* method to calculate the results. Zhu et al. [23] investigated the bending and vibration of CNT-reinforced thin and thick composite plates. They used FSDT and FEM in their studies. Mantari et al. [24] developed a novel shear deformation theory for composite plates where the shear correction factor is not required. They derived the governing equations of motion using the principle of virtual work and employed the Navier solutions to obtain the results. Fazzolari and Carrera [25, 26] investigated the vibration analysis of anisotropic multilayered plates and sandwich plates with anisotropic sheets including thermal effects and using the HTR formulation. Chen et al. [27] showed the sensitivity of the natural frequencies and buckling load of laminated composite plates to thermal stresses and initial stresses. Nedri et al. [28] studied the vibration of laminated composite plates resting on an elastic medium employing refined hyperbolic shear deformation theory. Li et al. [29] determined vibro-acoustic and buckling behaviors of fully clamped laminated composite plates with thermal effects. They applied CLT and FSDT to establish the model. Kiani [30] developed free vibration analysis of FG-CNT reinforced composite skew plates. They utilized FSDT to obtain the model and the Ritz method to obtain the results. Pingulkar and Suresha [31] developed natural frequency and mode shape analysis of cantilever laminated composite plates using the FEM with various fiber volume fractions. Zhang et al. [32] considered the vibration of

laminated composite plates with non-uniform BCs using an improved Fourier series method, and the results were verified by FEM data. Zamani et al. [33] considered the vibration analysis of viscoelastic composite plates. They employed higher-order shear deformation theory for a reinforced polymeric matrix on a visco-Pasternak foundation to extract the model and present closed form solutions for the transient response. Zhang and Selim [34] studied the free vibration of CNT reinforced laminated composite plates *using Reddy's* higher-order shear deformation theory. They applied the element-free IMLS-Ritz method to establish the results. Canales and Mantari [35] studied the free vibration of thick isotropic and laminated rectangular beams with arbitrary boundary conditions using the Carrera Unified Formulation and the Ritz method. They obtained accurate results for the first mode and validated these results using the 3D finite element solution. Chernikov et al. [36] presented an optimization problem of the dynamic response for an anisotropic composite plate using multi-field coupling with thermal constraints. They found optimal characteristics of an electro-magnetic field to reduce the amplitude of the plate vibrations. Fallah and Delzendeh [37] developed a novel meshless finite volume method with first order shear deformation theory to study vibrational behavior of laminated composite plates. Alaimo et al. [38] studied vibrational behavior of composite plates embedding viscoelastic layers. They developed layer-wise models of plates using the principle of virtual displacements and employed a Navier procedure to solve the problem. Zhang et al. [39] developed a novel exact solution for transverse vibration of rotationally-restrained orthotropic plates. They proposed a new formulation using the finite integral transform. Hachemi and Cherif [40] reported the free vibration investigation of composite laminated plate using higher-order shear deformation theory and a curved quadrilateral p-element. Tanzadeh and Amoushahi [41] considered various plate deformation theories to study the free vibration and buckling behavior of piezoelectric laminated composite plates. Vidal et al. [42] employed a variable separation method to investigate free vibration analysis of laminated composite plates. They used an iterative process to solve the non-linear problem. Faroughi et al. [43] employed NURBS-based isogeometric method to investigate the buckling and vibration and divergence analyses of anisotropic shells. They also applied a novel isogeometric higher-order shear deformation model to present the dynamic stability of anisotropic composite plates [44]. Safaei [45] investigated free vibrational analysis of laminated composite plates with a porous core. He applied first order shear deformation theory and FEM to solve the eigenvalue equation. Marchetti et al. [46] studied the dynamic behavior of sandwich structures and laminated composite

plates using an equivalent thin plate methodology with experimental validation. Sinha et al. [47] presented numerical and experimental investigation on vibration of woven glass fiber composite laminated plates. They employed an FFT analysis and an FE model in their study.

The investigation of the mechanical behavior of anti-symmetric laminated composite structures has been the subject of extensive research in recent years. Topal et al. [48] proposed a Teaching Learning Based Optimization (TLBO) to optimize the fundamental frequency of anti-symmetric laminated composite plates. They selected the fibre orientations of the layers as the optimization variables. They used the Artificial Bee Colony (ABC) algorithm to solve the problem. Narwariya et al. [49] developed a numerical study and harmonic analysis of free vibration for anti-symmetric cross-ply laminated composite plates. They employed FEM to determine the natural frequencies, mode shapes and harmonic analysis of anti-symmetric cross-ply laminated composite plates. Javed et al. [50] investigated the free vibrational behavior of symmetric and anti-symmetric cross-ply laminated composite plates. They considered higher-order shear deformation theory and a spline method to estimate the response for multi-layered plates under simply supported boundary conditions. Zhang et al. [51] presented the visco-elastic behavior of anti-symmetric laminated composites. They considered time and temperature dependent properties and employed classical lamination theory and Maxwell*'s* visco-elasticity model. Shukla et al. [52] employed a mesh-free approach using artificial intelligence and radial basis functions (RBF) to study the buckling analysis of symmetric and anti-symmetric laminated composite plates. Sahla et al. [53] investigated the vibration analysis of anti-symmetric laminated composites and soft core sandwich plates. They used a simple four-variable trigonometric shear deformation model and found an analytical solution. Belbachir et al. [54] addressed the bending response of anti-symmetric cross-ply laminated composite plates using a refined plate theory and a nonlinear thermo-mechanical loading model. The Navier solution was used to determine the results. Moreover, they developed a thermal flexural analysis of anti-symmetric cross-ply laminated plates [55]. Chai et al. [56] considered bistable anti-symmetric composite shells and presented a systematic study in hygrothermal environments to define the effect of temperature and moisture. They employed classical laminate theory and FEM simulation to extract the results. They also verified the theoretical results with experiments. Zhang et al. [57] predicted chaotic vibrations of a bi-stable asymmetric laminated composite square panel under foundation forces for the first time.

In the literature, many different applications for anti-symmetric laminated composite plates have been suggested and studied. Chattibi et al. [58] suggested their research is relevant to nuclear and aerospace engineering structures. The application of unsymmetric and anti-symmetric composite laminated plates have been reported in reconfigurable antenna [59], lightning striker [60], morphing structures [61] and stiffened plates with omega stringers [62]. For structures designed for dynamic control and stability with requirements such as high resonance frequency, vibration control and low centrifugal forces, the application of composite materials such as carbon/epoxy/graphite fiber reinforced polymers, can be a reliable choice [63].

Anti-symmetric laminated composite plates can be extensively used for many industrial applications and components such as fuselage structures, engine cowls, wing structures, flaps and aircraft access panels, which are surrounded by elastic media and exposed to temperature changes. Therefore, a comprehensive investigation of the vibration characteristics of anti-symmetric plates considering different lay-ups, the visco-elastic foundation, temperature effects and various boundary conditions is essential. However, according to the above literature review, the existing investigations on vibrational behavior of composite laminated plates do not include a comprehensive study for the combined effects of different anti-symmetric laminated arrangements, visco-elastic foundations, temperature and various boundary conditions. So, the deficiencies and shortcomings of previous studies are clear and studies including these aspects are necessary for safe and accurate design. Hence, in this study, the vibrational behavior analysis of anti-symmetric laminated composite plates resting on elastic foundations undergoing thermal effects is considered. In this comprehensive study, *Hamilton's principle and* higher-order shear deformation theory are employed to extract the governing equations of motion. A detailed numerical analysis using GDQM is performed for various temperatures, visco-elastic foundations, elastic properties, aspect and slenderness ratios, the arrangement of the anti-symmetric laminates and damping coefficients. Also, the results are extracted for different boundary conditions such as CCCC, SCCC, SCCS, SSCS and SSSS.

2. Formulation

2.1. Description

A multi-layered laminated composite plates resting on a Winkler-Pasternak foundation is considered taking into account thermal effects. as shown in Fig. 1.

2.2. Kinematics

Third Shear Deformation Theory (TSDT) is applied to present the kinematics model of plate resting on Winkler-Pasternak foundations. The displacement fields in third order shear deformation theory are:

$$u(x.y.z.t) = u_0(x.y.t) + z\phi_x(x.y.t) - \frac{4}{3h^2}z^3\left(\phi_x + \frac{\partial w_0}{\partial x}\right) \quad (1a)$$

$$v(x.y.z.t) = v_0(x.y.t) + z\phi_y(x.y.t) - \frac{4}{3h^2}z^3(\phi_y + \frac{\partial w_0}{\partial y}) \quad (1b)$$

$$w(x.y.z.t) = w_0(x.y.t) \quad (1c)$$

where $(u_0.v_0.w_0)$ are the displacements along the $(x.y.z)$ directions and $(\phi_x.\phi_y)$ indicate rotations about $(x.y)$, *respectively. The linear strains associated with Reddy's displacement fields* can be obtained as:

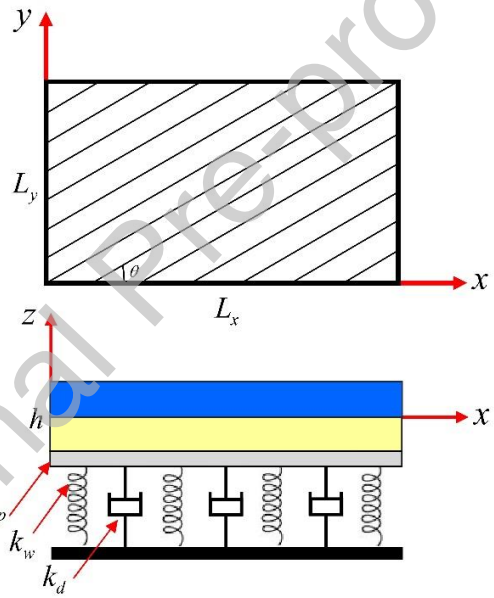

Fig. 1: Multi-layered laminated composite plate resting on a visco-elastic foundation

$$\varepsilon_{xx} = \frac{\partial u}{\partial x} = \frac{\partial u_0}{\partial x} + z\left(\frac{\partial \phi_x}{\partial x}\right) - c_1 z^3\left(\frac{\partial \phi_x}{\partial x} + \frac{\partial^2 w_0}{\partial x^2}\right) \quad (2a)$$

$$\varepsilon_{yy} = \frac{\partial v}{\partial y} = \frac{\partial v_0}{\partial y} + z\left(\frac{\partial \phi_y}{\partial y}\right) - c_1 z^3\left(\frac{\partial \phi_y}{\partial y} + \frac{\partial^2 w_0}{\partial y^2}\right) \quad (2b)$$

$$\gamma_{xy} = \frac{1}{2}\left(\frac{\partial u}{\partial y} + \frac{\partial v}{\partial x}\right) = \frac{\partial u_0}{\partial y} + \frac{\partial v_0}{\partial x} + z\left(\frac{\partial \phi_x}{\partial y} + \frac{\partial \phi_y}{\partial x}\right) - c_1 z^3\left(\frac{\partial \phi_x}{\partial y} + \frac{\partial \phi_y}{\partial x} + 2\frac{\partial^2 w_0}{\partial x \partial y}\right) \quad (2c)$$

$$\gamma_{xz} = \frac{1}{2}\left(\frac{\partial u}{\partial z} + \frac{\partial w}{\partial x}\right) = \phi_y + \frac{\partial w_0}{\partial y} - c_2 z^2\left(\phi_y + \frac{\partial w_0}{\partial y}\right) \quad (2d)$$

$$\gamma_{yz} = \frac{1}{2}\left(\frac{\partial v}{\partial z} + \frac{\partial w}{\partial y}\right) = \phi_x + \frac{\partial w_0}{\partial x} - c_2 z^2 \left(\phi_x + \frac{\partial w_0}{\partial x}\right) \tag{2e}$$

where $c_1 = \frac{4}{3h^2}$ and$c_2 = 3c_1$.

Eq. (2) can be rewritten as:

$$\begin{Bmatrix}\varepsilon_{xx}\\ \varepsilon_{yy}\\ \gamma_{xy}\end{Bmatrix} = \begin{Bmatrix}\varepsilon_{xx}^{(0)}\\ \varepsilon_{yy}^{(0)}\\ \gamma_{xy}^{(0)}\end{Bmatrix} + z\begin{Bmatrix}\varepsilon_{xx}^{(1)}\\ \varepsilon_{yy}^{(1)}\\ \gamma_{xy}^{(1)}\end{Bmatrix} + z^3\begin{Bmatrix}\varepsilon_{xx}^{(3)}\\ \varepsilon_{yy}^{(3)}\\ \gamma_{xy}^{(3)}\end{Bmatrix} \tag{3a}$$

$$\begin{Bmatrix}\gamma_{yz}\\ \gamma_{xz}\end{Bmatrix} = \begin{Bmatrix}\gamma_{yz}^{(0)}\\ \gamma_{xz}^{(0)}\end{Bmatrix} + z^2\begin{Bmatrix}\gamma_{yz}^{(2)}\\ \gamma_{xz}^{(2)}\end{Bmatrix} \tag{3b}$$

where the form of $\varepsilon_{xx}^{(0)}.\varepsilon_{xx}^{(1)}.\varepsilon_{xx}^{(3)}.\varepsilon_{yy}^{(0)}.\varepsilon_{yy}^{(1)}.\varepsilon_{yy}^{(3)}.\gamma_{xy}^{(0)}.\gamma_{xy}^{(1)}.\gamma_{xy}^{(3)}.\gamma_{xy}^{(1)}.\gamma_{xy}^{(2)}.\gamma_{xy}^{(1)}$ and $\gamma_{xy}^{(2)}$ are given in Appendix A.

2.3. Governing Equations of Motion

Using Hamilton principle, the governing equations of motion based on TSDT are extracted for laminated composite plates. Hamilton*'s* principle is given by:

$$H = \int_0^T (\delta\Pi_s + \delta\Pi_w - \delta\Pi_k)dt = 0 \tag{4}$$

where $\delta\Pi_s.\delta\Pi_w$ and $\delta\Pi_k$ are the first variation of the strain energy, virtual work which is done by the external forces and the kinetic energy, respectively and can be computed as:

$$\begin{aligned}\delta\Pi_s &= \int_v \left[\sigma_{xx}\delta\varepsilon_{xx} + \sigma_{yy}\delta\varepsilon_{yy} + \sigma_{xy}\delta\gamma_{xy} + \sigma_{xz}\delta\gamma_{xz} + \sigma_{yz}\delta\gamma_{yz}\right]dv \\ &= \int_A [N_{xx}\delta\varepsilon_{xx}^{(0)} + M_{xx}\delta\varepsilon_{xx}^{(1)} - c_1 P_{xx}\delta\varepsilon_{xx}^{(3)} + N_{yy}\delta\varepsilon_{yy}^{(0)} + M_{yy}\delta\varepsilon_{yy}^{(1)} - c_1 P_{yy}\delta\varepsilon_{yy}^{(3)} \\ &\quad + N_{xy}\delta\gamma_{xy}^{(0)} + M_{xy}\delta\gamma_{xy}^{(1)} - c_1 P_{xy}\delta\gamma_{xy}^{(3)} + Q_x\delta\gamma_{xz}^{(0)} - c_2 R_x\delta\gamma_{xz}^{(2)} - Q_y\delta\gamma_{yz}^{(0)} \\ &\quad - c_2 R_y\delta\gamma_{yz}^{(2)}]dxdz\end{aligned} \tag{5}$$

where:

$$(N_{ij}.M_{ij}.P_{ij}) = \int_{-\frac{h}{2}}^{\frac{h}{2}} \sigma_{ij}(1.z.z^3)dz \tag{6a}$$

$$(Q_i.R_i) = \int_{-\frac{h}{2}}^{\frac{h}{2}} \sigma_{iz}(1.z^2)dz \tag{6b}$$

In Eqs. (6), i and j take the symbols x and y.

Also:

$$\delta\Pi_k = \int_v \rho_0 \left[\left(\frac{\partial u_0}{\partial t} + z\frac{\partial \phi_x}{\partial t} - c_1 z^3\left(\frac{\partial \phi_x}{\partial t} + \frac{\partial^2 w_0}{\partial x \partial t}\right)\right)\left(\delta\left(\frac{\partial u_0}{\partial t}\right) + z\delta\left(\frac{\partial \phi_x}{\partial t}\right) - c_1 z^3 \delta\left(\frac{\partial \phi_x}{\partial t} + \frac{\partial^2 w_0}{\partial x \partial t}\right)\right) + \left(\frac{\partial v_0}{\partial t} + z\frac{\partial \phi_y}{\partial t} - c_1 z^3\left(\frac{\partial \phi_y}{\partial t} + \frac{\partial^2 w_0}{\partial x \partial t}\right)\right)\left(\delta\left(\frac{\partial v_0}{\partial t}\right) + z\delta\left(\frac{\partial \phi_y}{\partial t}\right) - c_1 z^3 \delta\left(\frac{\partial \phi_y}{\partial t} + \frac{\partial^2 w_0}{\partial x \partial t}\right)\right) + w_0 \delta w_0\right] dv$$

$$= \int_A \left[\left(m_0\frac{\partial u_0}{\partial t} + m_1\frac{\partial \phi_x}{\partial t} - c_1 m_3\left(\frac{\partial \phi_x}{\partial t} + \frac{\partial^2 w_0}{\partial x \partial t}\right)\right)\delta\left(\frac{\partial u_0}{\partial t}\right) + \left(m_1\frac{\partial u_0}{\partial t} + m_2\frac{\partial \phi_x}{\partial t} - c_1 m_4\left(\frac{\partial \phi_x}{\partial t} + \frac{\partial^2 w_0}{\partial x \partial t}\right)\right)\delta\left(\frac{\partial \phi_x}{\partial t}\right) - c_1\left(m_3\frac{\partial u_0}{\partial t} + m_4\frac{\partial \phi_x}{\partial t} - c_1 m_6\left(\frac{\partial \phi_x}{\partial t} + \frac{\partial^2 w_0}{\partial x \partial t}\right)\right)\delta\left(\frac{\partial \phi_x}{\partial t} + \frac{\partial^2 w_0}{\partial x \partial t}\right) + \left(m_0\frac{\partial v_0}{\partial t} + m_1\frac{\partial \phi_y}{\partial t} - c_1 m_3\left(\frac{\partial \phi_y}{\partial t} + \frac{\partial^2 w_0}{\partial x \partial t}\right)\right)\delta\left(\frac{\partial v_0}{\partial t}\right) + \left(m_1\frac{\partial v_0}{\partial t} + m_2\frac{\partial \phi_y}{\partial t} - c_1 m_4\left(\frac{\partial \phi_y}{\partial t} + \frac{\partial^2 w_0}{\partial x \partial t}\right)\right)\delta\left(\frac{\partial \phi_y}{\partial t}\right) - c_1\left(m_3\frac{\partial v_0}{\partial t} + m_4\frac{\partial \phi_y}{\partial t} - c_1 m_6\left(\frac{\partial \phi_y}{\partial t} + \frac{\partial^2 w_0}{\partial x \partial t}\right)\right)\delta\left(\frac{\partial \phi_y}{\partial t} + \frac{\partial^2 w_0}{\partial x \partial t}\right)\right] dxdy \quad (7)$$

where $m_i = \int_{-\frac{h}{2}}^{\frac{h}{2}} \rho_0 (z)^i dz$ and for multi-layered laminated composite is equal to:

$$m_i = \sum_{k=1}^{n} \int_{z_k}^{z_{k+1}} \rho^{(k)} (z)^i dz \quad (i = 0.1.2. \ldots .6) \quad (8)$$

where n is number of layers. Moreover, for external forces the variation of virtual work can be considered as:

$$\delta\Pi_w = \int_A \left[\left(q + K_w w_0 + K_p\left(\frac{\partial^2 w_0}{\partial x^2} + \frac{\partial^2 w_0}{\partial y^2}\right) + K_d\frac{\partial w_0}{\partial t}\right)\delta w_0\right] dxdy \quad (9)$$

where q is transverse distributed force of laminate and K_w, K_p and K_d are the Winkler, Pasternak and damping coefficients due to the visco-elastic foundation, respectively.

By substituting Eqs. (5), (7) and (9) into (4) and using some algebraic simplifications, the equations of motion are generated as:

$$\delta u_0: \quad \frac{\partial N_{xx}}{\partial x}+\frac{\partial N_{xy}}{\partial y}=m_0\ddot{u}_0+\bar{m}_1\ddot{\phi}_x-c_1m_3\frac{\partial \ddot{w}_0}{\partial x} \tag{10a}$$

$$\delta v_0: \quad \frac{\partial N_{xy}}{\partial x}+\frac{\partial N_{yy}}{\partial y}=m_0\ddot{v}_0+\bar{m}_1\ddot{\phi}_y-c_1m_3\frac{\partial \ddot{w}_0}{\partial y} \tag{10b}$$

$$\delta w_0: \quad \frac{\partial}{\partial x}(Q_x-c_2R_x)+\frac{\partial}{\partial y}\left(Q_y-c_2R_y\right)+\frac{\partial}{\partial x}\left(N_{xx}\frac{\partial w_0}{\partial x}+N_{xy}\frac{\partial w_0}{\partial y}\right)+\frac{\partial}{\partial y}\left(N_{xy}\frac{\partial w_0}{\partial x}+N_{yy}\frac{\partial w_0}{\partial y}\right)+c_1\left(\frac{\partial^2P_{xx}}{\partial x^2}+2\frac{\partial^2P_{xy}}{\partial x\partial y}+\frac{\partial^2P_{yy}}{\partial y^2}\right)+q+K_ww_0+K_p\left(\frac{\partial^2w_0}{\partial x^2}+\frac{\partial^2w_0}{\partial y^2}\right)+K_d\frac{\partial w_0}{\partial t}=m_0\ddot{w}_0-c_1^2m_6(\frac{\partial^2\ddot{w}_0}{\partial x^2}+\frac{\partial^2\ddot{w}_0}{\partial y^2})+c_1\left[m_3\left(\frac{\partial\ddot{u}_0}{\partial x}+\frac{\partial\ddot{v}_0}{\partial y}\right)+\bar{m}_4\left(\frac{\partial\ddot{\phi}_x}{\partial x}+\frac{\partial\ddot{\phi}_y}{\partial y}\right)\right] \tag{10c}$$

$$\delta\phi_x: \quad \frac{\partial}{\partial x}(M_{xx}-c_1P_{xx})+\frac{\partial}{\partial y}(M_{xy}-c_1P_{xy})-(Q_x-c_2R_x)=\bar{m}_1\ddot{u}_0+\bar{\bar{m}}_2\ddot{\phi}_x-c_1\bar{m}_4\frac{\partial\ddot{w}_0}{\partial x} \tag{10d}$$

$$\delta\phi_y: \quad \frac{\partial}{\partial x}(M_{xy}-c_1P_{xy})+\frac{\partial}{\partial y}(M_{yy}-c_1P_{yy})-(Q_y-c_2R_y)=\bar{m}_1\ddot{v}_0+\bar{\bar{m}}_2\ddot{\phi}_y-c_1\bar{m}_4\frac{\partial\ddot{w}_0}{\partial y} \tag{10e}$$

where:

$$m_i=\int_{-\frac{h}{2}}^{\frac{h}{2}}\rho_0\,(z)^i dz=\sum_{K=1}^{n}\int_{z_k}^{z_k+1}\rho^{(k)}(z)^i dz \qquad (i=0.1.2.\ldots.6) \tag{11a}$$

$$\bar{m}_i=m_i-c_1m_{i+2} \tag{11b}$$

$$\bar{\bar{m}}_2=m_2-2c_1m_4+c_1^2m_6 \tag{11c}$$

In addition, the stress resultants in terms of strains can be written as:

$$\begin{Bmatrix}\{N\}\\ \{M\}\\ \{P\}\end{Bmatrix}=\begin{bmatrix}[A] & [B] & [E]\\ [B] & [D] & [F]\\ [E] & [F] & [H]\end{bmatrix}\begin{Bmatrix}\{\varepsilon^{(0)}\}\\ \{\varepsilon^{(1)}\}\\ \{\varepsilon^{(3)}\}\end{Bmatrix}-\begin{Bmatrix}\{N^T\}\\ \{M^T\}\\ \{P^T\}\end{Bmatrix} \tag{12}$$

$$\begin{Bmatrix}\{Q\}\\ \{R\}\end{Bmatrix}=\begin{bmatrix}[A] & [D]\\ [D] & [F]\end{bmatrix}\begin{Bmatrix}\{\gamma^{(0)}\}\\ \{\gamma^{(2)}\}\end{Bmatrix} \tag{13}$$

where $\{N\}.\{M\}.\{P\}$ are defined by Eq. (6a) as 3×1 vectors and $\{Q\},\{R\}$ are 2×1 vectors expressed by Eq. (6b). Also, $\{N^T\},\{M^T\},\{P^T\}$ are the thermal stress resultants that are described as:

$$\{N^T\}=\begin{Bmatrix}N_{xx}^T\\ N_{yy}^T\\ N_{xy}^T\end{Bmatrix}=\sum_{k=1}^{n}\int_{z_k}^{z_k+1}[\bar{Q}]^k\begin{Bmatrix}\alpha_{xx}\\ \alpha_{yy}\\ 2\alpha_{xy}\end{Bmatrix}^k\Delta T\,dz \tag{14a}$$

$$\{M^T\}=\begin{Bmatrix}M_{xx}^T\\ M_{yy}^T\\ M_{xy}^T\end{Bmatrix}=\sum_{k=1}^{n}\int_{z_k}^{z_k+1}[\bar{Q}]^k\begin{Bmatrix}\alpha_{xx}\\ \alpha_{yy}\\ 2\alpha_{xy}\end{Bmatrix}^k\Delta T\,zdz \tag{14b}$$

$$\{P^T\} = \begin{Bmatrix} P_{xx}^T \\ P_{yy}^T \\ P_{xy}^T \end{Bmatrix} = \sum_{k=1}^{n} \int_{z_k}^{z_{k+1}} [\bar{Q}]^k \begin{Bmatrix} \alpha_{xx} \\ \alpha_{yy} \\ 2\alpha_{xy} \end{Bmatrix}^k \Delta T \, z^3 dz \tag{14c}$$

where $[\bar{Q}]^k$ and $\{\alpha_{ij}\}^k$ are the 3×3 transformed reduced stiffness coefficients matrix and the 3×1 vector of thermal expansion coefficients for the k^{th} layer respectively, and presented in Appendix B. Also, ΔT is the thermal field which assumed as uniform in current work.

In addition, $[A], [B], [D], [E], [F]$ and $[H]$ are defined as:

$$A_{ij} = \sum_{k=1}^{N} \bar{Q}_{ij}^{(k)} (z_{k+1} - z_k) \;\; ; \; B_{ij} = \frac{1}{2} \sum_{k=1}^{N} \bar{Q}_{ij}^{(k)} (z_{k+1}^2 - z_k^2)$$

$$D_{ij} = \frac{1}{3} \sum_{k=1}^{N} \bar{Q}_{ij}^{(k)} (z_{k+1}^3 - z_k^3) \; ; \; E_{ij} = \frac{1}{4} \sum_{k=1}^{N} \bar{Q}_{ij}^{(k)} [(z_{k+1})^4 - (z_k)^4] \tag{15}$$

$$F_{ij} = \frac{1}{5} \sum_{k=1}^{N} \bar{Q}_{ij}^{(k)} [(z_{k+1})^5 - (z_k)^5] \; ; \; H_{ij} = \frac{1}{7} \sum_{k=1}^{N} \bar{Q}_{ij}^{(k)} [(z_{k+1})^7 - (z_k)^7]$$

For Eq. (12), $(i, j = 1,2,6)$ and for Eq. (13), $(i, j = 4,5)$. Eqs. (12) and (13) are given in detail in Appendix C.

By substituting Eqs. (12) and (13) into Eqs. (10) and considering Eqs. (14)-(15) and Appendices A, B and C, the equations of motion can be derived in terms of the displacement as:

$$A_{11} \frac{\partial^2 u_0}{\partial x^2} + 2A_{16} \frac{\partial^2 u_0}{\partial x \partial y} + A_{66} \frac{\partial^2 u_0}{\partial y^2} + A_{16} \frac{\partial^2 v_0}{\partial x^2} + (A_{12} + A_{66}) \frac{\partial^2 v_0}{\partial x \partial y} + A_{26} \frac{\partial^2 v_0}{\partial y^2} - c_1 E_{11} \frac{\partial^3 w_0}{\partial x^3} - (c_1 E_{12} + 2c_1 E_{66}) \frac{\partial^3 w_0}{\partial y^2 \partial x} - 3c_1 E_{16} \frac{\partial^3 w_0}{\partial x^2 \partial y} - c_1 E_{26} \frac{\partial^3 w_0}{\partial y^3} + \bar{B}_{11} \frac{\partial^2 \phi_x}{\partial x^2} + 2\bar{B}_{16} \frac{\partial^2 \phi_x}{\partial x \partial y} + \bar{B}_{66} \frac{\partial^2 \phi_x}{\partial y^2} + \bar{B}_{16} \frac{\partial^2 \phi_y}{\partial x^2} + [\bar{B}_{12} + \bar{B}_{66}] \frac{\partial^2 \phi_y}{\partial x \partial y} + \bar{B}_{26} \frac{\partial^2 \phi_y}{\partial y^2} - \frac{\partial N_{xx}^T}{\partial x} - \frac{\partial N_{xy}^T}{\partial y} = m_0 \ddot{u}_0 + \bar{m}_1 \ddot{\phi}_x - c_1 m_3 \frac{\partial \ddot{w}_0}{\partial x} \tag{16a}$$

$$A_{16} \frac{\partial^2 u_0}{\partial x^2} + (A_{12} + A_{66}) \frac{\partial^2 u_0}{\partial x \partial y} + A_{26} \frac{\partial^2 u_0}{\partial y^2} + A_{66} \frac{\partial^2 v_0}{\partial x^2} + 2A_{26} \frac{\partial^2 v_0}{\partial x \partial y} + A_{22} \frac{\partial^2 v_0}{\partial y^2} - c_1 E_{16} \frac{\partial^3 w_0}{\partial x^3} - 3c_1 E_{26} \frac{\partial^3 w_0}{\partial y^2 \partial x} - (c_1 E_{12} + 2c_1 E_{66}) \frac{\partial^3 w_0}{\partial x^2 \partial y} - c_1 E_{22} \frac{\partial^3 w_0}{\partial y^3} + \bar{B}_{16} \frac{\partial^2 \phi_x}{\partial x^2} + [\bar{B}_{12} + \bar{B}_{66}] \frac{\partial^2 \phi_x}{\partial x \partial y} + \bar{B}_{26} \frac{\partial^2 \phi_x}{\partial y^2} + \bar{B}_{66} \frac{\partial^2 \phi_y}{\partial x^2} + 2\bar{B}_{26} \frac{\partial^2 \phi_y}{\partial x \partial y} + \bar{B}_{22} \frac{\partial^2 \phi_y}{\partial y^2} - \frac{\partial N_{xy}^T}{\partial x} - \frac{\partial N_{yy}^T}{\partial y} = m_0 \ddot{v}_0 + \bar{m}_1 \ddot{\phi}_y - c_1 m_3 \frac{\partial \ddot{w}_0}{\partial y} \tag{16b}$$

$$c_1 E_{11} \frac{\partial^3 u_0}{\partial x^3} + 3c_1 E_{16} \frac{\partial^3 u_0}{\partial x^2 \partial y} + (c_1 E_{12} + 2c_1 E_{66}) \frac{\partial^3 u_0}{\partial y^2 \partial x} + c_1 E_{26} \frac{\partial^3 u_0}{\partial y^3} + c_1 E_{16} \frac{\partial^3 v_0}{\partial x^3} + (c_1 E_{12} + 2c_1 E_{66}) \frac{\partial^3 v_0}{\partial x^2 \partial y} + 3c_1 E_{26} \frac{\partial^3 v_0}{\partial y^2 \partial x} + c_1 E_{22} \frac{\partial^3 v_0}{\partial y^3} - c_1^2 H_{11} \frac{\partial^4 w_0}{\partial x^4} - 4c_1^2 H_{16} \frac{\partial^4 w_0}{\partial x^3 \partial y} - 4c_1^2 H_{26} \frac{\partial^4 w_0}{\partial y^3 \partial x} - 2c_1^2 (H_{12} + 2H_{66}) \frac{\partial^4 w_0}{\partial y^2 \partial x^2} - c_1^2 H_{22} \frac{\partial^4 w_0}{\partial y^4} + c_1 \bar{F}_{11} \frac{\partial^3 \phi_x}{\partial x^3} + 3c_1 \bar{F}_{16} \frac{\partial^3 \phi_x}{\partial x^2 \partial y} + c_1 [\bar{F}_{12} + 2\bar{F}_{66}] \frac{\partial^3 \phi_x}{\partial y^2 \partial x} + c_1 \bar{F}_{26} \frac{\partial^3 \phi_x}{\partial y^3} + c_1 \bar{F}_{16} \frac{\partial^3 \phi_y}{\partial x^3} + 3c_1 \bar{F}_{26} \frac{\partial^3 \phi_y}{\partial x \partial y^2} + c_1 [\bar{F}_{12} + 2\bar{F}_{66}] \frac{\partial^3 \phi_y}{\partial x^2 \partial y} + c_1 \bar{F}_{22} \frac{\partial^3 \phi_y}{\partial y^3} + \bar{\bar{A}}_{45} [\frac{\partial \phi_y}{\partial x} + \frac{\partial \phi_x}{\partial y} + 2 \frac{\partial^2 w_0}{\partial x \partial y}] + \bar{\bar{A}}_{44} [\frac{\partial \phi_y}{\partial y} + \frac{\partial^2 w_0}{\partial y^2}] + \bar{\bar{A}}_{55} [\frac{\partial \phi_x}{\partial x} + \frac{\partial^2 w_0}{\partial x^2}] - N_{xx}^T \frac{\partial^2 w_0}{\partial x^2} - 2N_{xy}^T \frac{\partial^2 w_0}{\partial x \partial y} - N_{yy}^T \frac{\partial^2 w_0}{\partial y^2} - c_1 (\frac{\partial^2 P_{xx}^T}{\partial x^2} + 2 \frac{\partial^2 P_{xy}^T}{\partial x \partial y} + \frac{\partial^2 P_{yy}^T}{\partial y^2}) + K_p (\frac{\partial^2 w_0}{\partial x^2} + \frac{\partial^2 w_0}{\partial y^2}) + K_w w_0 + q + K_d \frac{\partial w_0}{\partial t} = m_0 \ddot{w}_0 - c_1^2 m_6 (\frac{\partial^2 \ddot{w}_0}{\partial x^2} + \frac{\partial^2 \ddot{w}_0}{\partial y^2}) + c_1 \left[m_3 \left(\frac{\partial \ddot{u}_0}{\partial x} + \frac{\partial \ddot{v}_0}{\partial y} \right) + \bar{m}_4 \left(\frac{\partial \ddot{\phi}_x}{\partial x} + \frac{\partial \ddot{\phi}_y}{\partial y} \right) \right] \tag{16c}$$

$$\bar{B}_{11}\frac{\partial^2 u_0}{\partial x^2}+2\bar{B}_{16}\frac{\partial^2 u_0}{\partial x\partial y}+\bar{B}_{66}\frac{\partial^2 u_0}{\partial y^2}+\bar{B}_{16}\frac{\partial^2 v_0}{\partial x^2}+\left[\bar{B}_{12}+\bar{B}_{66}\right]\frac{\partial^2 v_0}{\partial x\partial y}+\bar{B}_{26}\frac{\partial^2 v_0}{\partial y^2}-c_1\bar{F}_{11}\frac{\partial^3 w_0}{\partial x^3}-$$
$$3c_1\bar{F}_{16}\frac{\partial^3 w_0}{\partial x^2\partial y}-c_1\left[\bar{F}_{12}+2\bar{F}_{66}\right]\frac{\partial^3 w_0}{\partial y^2\partial x}-c_1\bar{F}_{26}\frac{\partial^3 w_0}{\partial y^3}+\bar{\bar{D}}_{11}\frac{\partial^2\phi_x}{\partial x^2}+2\bar{\bar{D}}_{16}\frac{\partial^2\phi_x}{\partial x\partial y}+\bar{\bar{D}}_{66}\frac{\partial^2\phi_x}{\partial y^2}+\bar{\bar{D}}_{16}\frac{\partial^2\phi_y}{\partial x^2}+$$
$$\left[\bar{\bar{D}}_{12}+\bar{\bar{D}}_{66}\right]\frac{\partial^2\phi_y}{\partial x\partial y}+\bar{\bar{D}}_{26}\frac{\partial^2\phi_y}{\partial y^2}-\bar{\bar{A}}_{45}\left[\phi_y+\frac{\partial w_0}{\partial y}\right]-\bar{\bar{A}}_{55}\left[\phi_x+\frac{\partial w_0}{\partial x}\right]-\frac{\partial M_{xx}^T}{\partial x}-\frac{\partial M_{xy}^T}{\partial y}+c_1\left(\frac{\partial P_{xx}^T}{\partial x}+\frac{\partial P_{xy}^T}{\partial y}\right)=$$
$$\bar{m}_1\ddot{u}_0+\bar{\bar{m}}_2\ddot{\phi}_x-c_1\bar{m}_4\frac{\partial\ddot{w}_0}{\partial x} \tag{16d}$$

$$\bar{B}_{16}\frac{\partial^2 u_0}{\partial x^2}+\left[\bar{B}_{12}+\bar{B}_{66}\right]\frac{\partial^2 u_0}{\partial x\partial y}+\bar{B}_{26}\frac{\partial^2 u_0}{\partial y^2}+\bar{B}_{66}\frac{\partial^2 v_0}{\partial x^2}+2\bar{B}_{26}\frac{\partial^2 v_0}{\partial x\partial y}+\bar{B}_{22}\frac{\partial^2 v_0}{\partial y^2}+-c_1\bar{F}_{16}\frac{\partial^3 w_0}{\partial x^3}-$$
$$c_1[\bar{F}_{12}+2\bar{F}_{66}]\frac{\partial^3 w_0}{\partial x^2\partial y}-3c_1\bar{F}_{26}\frac{\partial^3 w_0}{\partial y^2\partial x}-c_1\bar{F}_{22}\frac{\partial^3 w_0}{\partial y^3}+\bar{\bar{D}}_{16}\frac{\partial^2\phi_x}{\partial x^2}+\left[\bar{\bar{D}}_{12}+\bar{\bar{D}}_{66}\right]\frac{\partial^2\phi_x}{\partial x\partial y}+\bar{\bar{D}}_{26}\frac{\partial^2\phi_x}{\partial y^2}+$$
$$\bar{\bar{D}}_{66}\frac{\partial^2\phi_y}{\partial x^2}+2\bar{\bar{D}}_{26}\frac{\partial^2\phi_y}{\partial x\partial y}+\bar{\bar{D}}_{22}\frac{\partial^2\phi_y}{\partial y^2}-\bar{\bar{A}}_{44}[\phi_y+\frac{\partial w_0}{\partial y}]-\bar{\bar{A}}_{45}[\phi_x+\frac{\partial w_0}{\partial x}]-\frac{\partial M_{xy}^T}{\partial x}-\frac{\partial M_{yy}^T}{\partial y}+c_1\left(\frac{\partial P_{xy}^T}{\partial x}+\frac{\partial P_{yy}^T}{\partial y}\right)=$$
$$\bar{m}_1\ddot{v}_0+\bar{\bar{m}}_2\ddot{\phi}_y-c_1\bar{m}_4\frac{\partial\ddot{w}_0}{\partial y} \tag{16e}$$

where:

$$\bar{B}_{ij}=B_{ij}-c_1E_{ij}\quad;\quad\bar{F}_{ij}=F_{ij}-c_1H_{ij}$$
$$\bar{\bar{D}}_{ij}=D_{ij}-2c_1F_{ij}+c_1^2H_{ij}\quad;\quad\bar{\bar{A}}_{ij}=A_{ij}-2c_2D_{ij}+c_2^2F_{ij} \tag{17}$$

Also, the mathematical forms for simply supported (SS) and clamped (C) boundary conditions, which are the most common for plates, are:

$$SS:\begin{cases}u_0=w_0=\phi_x=0 & \text{at } x=0.L_x\\ v_0=w_0=\phi_y=0 & \text{at } y=0.L_y\end{cases} \tag{18a}$$

$$C:\begin{cases}u_0=w_0=w_{0.x}=\phi_x=\phi_y=0 & \text{at } x=0.L_x\\ v_0=w_0=w_{0.y}=\phi_x=\phi_y=0 & \text{at } y=0.L_y\end{cases} \tag{18b}$$

3. Solution Procedure

In this section, the governing equations of motion presented in Eqs. (16) are solved using the generalized differential quadrature method (GDQM). The GDQM is a numerical technique used to solve IVPs and BVPs. The GDQM is an alternative to the other numerical methods such as the finite element method (FEM) and the finite difference method (FDM). The GDQM employs some weighting coefficients to transform the IVPs and BVPs to a system of algebraic equations which has a straight forward solution. To this end, the domain of the problem is divided into sufficient mesh points and then the first and high order derivatives of a function at each mesh point can be approximated.

3.1. Differential Quadrature Method

In the current work, the differential quadrature method (DQM) as an effective and strong numerical solution is employed to solve the vibration problem of anti-symmetric laminated composite plates. Based on the DQM, the domain of the composite plate is discretized into $N_x \times N_y$ mesh points in the x and y directions respectively. Here, to generate the mesh points the Chebyshev–Gauss–Lobatto distribution is employed, which is given by:

$$x_i = \frac{1}{2}\left(1-\cos\left(\frac{i-1}{N_x-1}\pi\right)\right) \qquad i=1,...,N_x \tag{19a}$$

$$y_j = \frac{1}{2}\left(1-\cos\left(\frac{j-1}{N_y-1}\pi\right)\right) \qquad j=1,...,N_y \tag{19b}$$

To implement the DQM, all of the derivatives of $f(x,y)$, as a two dimensional function at each mesh point (x_i, y_i), are defined via a weighted linear summation as:

$$\left.\frac{\partial^n f(x,y)}{\partial x^n}\right|_{(x_i,y_j)} = \sum_{k=1}^{N_x} \Lambda_{ik}^{x(n)} f(x_k, y_j) \tag{20a}$$

$$\left.\frac{\partial^m f(x,y)}{\partial y^m}\right|_{(x_i,y_j)} = \sum_{l=1}^{N_y} \Lambda_{jl}^{y(m)} f(x_i, y_l) \tag{20b}$$

$$\left.\frac{\partial^{n+m} f(x,y)}{\partial x^n \partial y^m}\right|_{(x_i,y_j)} = \sum_{k=1}^{N_x}\sum_{l=1}^{N_y} \Lambda_{ik}^{x(n)} \Lambda_{jl}^{y(m)} f(x_k, y_l) \tag{20c}$$

where $i=1,..,N_x$, $j=1,..,N_y$ and $\Lambda_{ik}^{x(n)}$, $\Lambda_{jl}^{y(m)}$ are weighting coefficients relevant to the n^{th} and m^{th} order derivatives with respect to the x and y directions respectively. The weighting coefficients for the first order derivative with respect to x are given by [64]:

$$\Lambda_{ik}^{x(1)} = \begin{cases} \dfrac{M(x_i)}{(x_i - x_k)M(x_k)} & for\ i \neq k \\ -\displaystyle\sum_{\substack{k=1 \\ i\neq k}}^{N_x} \Lambda_{ik}^{x(1)} & for\ i = k \end{cases} \tag{21}$$

where $M(x_i)$ is the Lagrangian polynomial:

$$M(x_i) = \prod_{\substack{k=1 \\ i\neq k}}^{N_x} (x_i - x_k) \tag{22}$$

The weighting coefficients for high order derivatives can be calculated as:

$$\Lambda_{ik}^{x(2)} = \sum_{p=1}^{N_x} \Lambda_{ip}^{x(1)} \Lambda_{pk}^{x(1)} \tag{23a}$$

$$\Lambda_{ik}^{x(3)} = \sum_{p=1}^{N_x} \Lambda_{ip}^{x(1)} \Lambda_{pk}^{x(2)} \tag{23b}$$

$$\Lambda_{ik}^{x(4)} = \sum_{p=1}^{N_x} \Lambda_{ip}^{x(1)} \Lambda_{pk}^{x(3)} \tag{23c}$$

In the same way, $\Lambda_{ik}^{y(m)}$ can be determined by substitution of variable y and subscripts j, l where *m* denotes the order of derivative.

Using DQM principles, the governing equations of motion (Eqs. (16)) are discretized in the following form:

$$\begin{aligned}
&A_{11}\sum_{k=1}^{N_x}\Lambda_{ik}^{x(2)}(u_0)_{kj} + 2A_{16}\sum_{k=1}^{N_x}\sum_{l=1}^{N_y}\Lambda_{ik}^{x(1)}\Lambda_{jl}^{y(1)}(u_0)_{kl} + A_{66}\sum_{k=1}^{N_y}\Lambda_{jl}^{y(2)}(u_0)_{il} + A_{16}\sum_{k=1}^{N_x}\Lambda_{ik}^{x(2)}(v_0)_{kj} \\
&+ (A_{12}+A_{66})\sum_{k=1}^{N_x}\sum_{l=1}^{N_y}\Lambda_{ik}^{x(1)}\Lambda_{jl}^{y(1)}(v_0)_{kl} + A_{26}\sum_{k=1}^{N_y}\Lambda_{jl}^{y(2)}(v_0)_{il} - c_1E_{11}\sum_{k=1}^{N_x}\Lambda_{ik}^{x(3)}(w_0)_{kj} \\
&- (c_1E_{12}+2c_1E_{66})\sum_{k=1}^{N_x}\sum_{l=1}^{N_y}\Lambda_{ik}^{x(1)}\Lambda_{jl}^{y(2)}(w_0)_{kl} - 3c_1E_{16}\sum_{k=1}^{N_x}\sum_{l=1}^{N_y}\Lambda_{ik}^{x(2)}\Lambda_{jl}^{y(1)}(w_0)_{kl} \\
&- c_1E_{26}\sum_{k=1}^{N_y}\Lambda_{jl}^{y(3)}(w_0)_{il} + \bar{B}_{11}\sum_{k=1}^{N_x}\Lambda_{ik}^{x(2)}(\phi_x)_{kj} + 2\bar{B}_{16}\sum_{k=1}^{N_x}\sum_{l=1}^{N_y}\Lambda_{ik}^{x(1)}\Lambda_{jl}^{y(1)}(\phi_x)_{kl} \\
&+ \bar{B}_{66}\sum_{k=1}^{N_y}\Lambda_{jl}^{y(2)}(\phi_x)_{il} + \bar{B}_{16}\sum_{k=1}^{N_x}\Lambda_{ik}^{x(2)}(\phi_y)_{kj} + [\bar{B}_{12}+\bar{B}_{66}]\sum_{k=1}^{N_x}\sum_{l=1}^{N_y}\Lambda_{ik}^{x(1)}\Lambda_{jl}^{y(1)}(\phi_y)_{kl} \\
&+ \bar{B}_{26}\sum_{k=1}^{N_y}\Lambda_{jl}^{y(2)}(\phi_y)_{il} = -\omega^2\left[m_0(u_0)_{ij} + \bar{m}_1(\phi_x)_{ij} - c_1m_3\sum_{k=1}^{N_x}\Lambda_{ik}^{x(1)}(w_0)_{kj}\right]
\end{aligned} \tag{24a}$$

$$A_{16}\sum_{k=1}^{N_x}\Lambda_{ik}^{x(2)}(u_0)_{kj}+(A_{12}+A_{66})\sum_{k=1}^{N_x}\sum_{l=1}^{N_y}\Lambda_{ik}^{x(1)}\Lambda_{jl}^{y(1)}(u_0)_{kl}+A_{26}\sum_{k=1}^{N_y}\Lambda_{jl}^{y(2)}(u_0)_{il}$$
$$+A_{66}\sum_{k=1}^{N_x}\Lambda_{ik}^{x(2)}(v_0)_{kj}+2A_{26}\sum_{k=1}^{N_x}\sum_{l=1}^{N_y}\Lambda_{ik}^{x(1)}\Lambda_{jl}^{y(1)}(v_0)_{kl}+A_{22}\sum_{k=1}^{N_y}\Lambda_{jl}^{y(2)}(v_0)_{il}$$
$$-c_1E_{16}\sum_{k=1}^{N_x}\Lambda_{ik}^{x(3)}(w_0)_{kj}-3c_1E_{26}\sum_{k=1}^{N_x}\sum_{l=1}^{N_y}\Lambda_{ik}^{x(1)}\Lambda_{jl}^{y(2)}(w_0)_{kl}$$
$$-(c_1E_{12}+2c_1E_{66})\sum_{k=1}^{N_x}\sum_{l=1}^{N_y}\Lambda_{ik}^{x(2)}\Lambda_{jl}^{y(1)}(w_0)_{kl}-c_1E_{22}\sum_{k=1}^{N_y}\Lambda_{jl}^{y(3)}(w_0)_{il}$$
$$+\bar{B}_{16}\sum_{k=1}^{N_x}\Lambda_{ik}^{x(2)}(\phi_x)_{kj}+[\bar{B}_{12}+\bar{B}_{66}]\sum_{k=1}^{N_x}\sum_{l=1}^{N_y}\Lambda_{ik}^{x(1)}\Lambda_{jl}^{y(1)}(\phi_x)_{kl}+\bar{B}_{26}\sum_{k=1}^{N_y}\Lambda_{jl}^{y(2)}(\phi_x)_{il}$$
$$+\bar{B}_{66}\sum_{k=1}^{N_x}\Lambda_{ik}^{x(2)}(\phi_y)_{kj}+2\bar{B}_{16}\sum_{k=1}^{N_x}\sum_{l=1}^{N_y}\Lambda_{ik}^{x(1)}\Lambda_{jl}^{y(1)}(\phi_y)_{kl}+\bar{B}_{22}\sum_{k=1}^{N_y}\Lambda_{jl}^{y(2)}(\phi_y)_{il}$$
$$=-\omega^2\left[m_0(v_0)_{ij}+\bar{m}_1(\phi_y)_{ij}-c_1m_3\sum_{k=1}^{N_y}\Lambda_{ik}^{y(1)}(w_0)_{kj}\right] \tag{24b}$$

$$
\begin{aligned}
&c_1E_{11}\sum_{k=1}^{N_x}\Lambda_{ik}^{x(3)}(u_0)_{kj}+3c_1E_{16}\sum_{k=1}^{N_x}\sum_{l=1}^{N_y}\Lambda_{ik}^{x(2)}\Lambda_{jl}^{y(1)}(u_0)_{kl}+(c_1E_{12}+2c_1E_{66})\sum_{k=1}^{N_x}\sum_{l=1}^{N_y}\Lambda_{ik}^{x(1)}\Lambda_{jl}^{y(2)}(u_0)_{kl}\\
&\quad+c_1E_{26}\sum_{k=1}^{N_y}\Lambda_{jl}^{y(3)}(u_0)_{il}+c_1E_{16}\sum_{k=1}^{N_x}\Lambda_{ik}^{x(3)}(v_0)_{kj}\\
&\quad+(c_1E_{12}+2c_1E_{66})\sum_{k=1}^{N_x}\sum_{l=1}^{N_y}\Lambda_{ik}^{x(2)}\Lambda_{jl}^{y1}(v_0)_{kl}+3c_1E_{26}\sum_{k=1}^{N_x}\sum_{l=1}^{N_y}\Lambda_{ik}^{x(1)}\Lambda_{jl}^{y(2)}(v_0)_{kl}\\
&\quad+c_1E_{22}\sum_{k=1}^{N_y}\Lambda_{jl}^{y(3)}(v_0)_{il}-c_1^2H_{11}\sum_{k=1}^{N_x}\Lambda_{ik}^{x(4)}(w_0)_{kj}-4c_1^2H_{16}\sum_{k=1}^{N_x}\sum_{l=1}^{N_y}\Lambda_{ik}^{x(3)}\Lambda_{jl}^{y(1)}(w_0)_{kl}\\
&\quad-4c_1^2H_{26}\sum_{k=1}^{N_x}\sum_{l=1}^{N_y}\Lambda_{ik}^{x(1)}\Lambda_{jl}^{y(3)}(w_0)_{kl}-2c_1^2(H_{12}+2H_{66})\sum_{k=1}^{N_x}\sum_{l=1}^{N_y}\Lambda_{ik}^{x(2)}\Lambda_{jl}^{y(2)}(w_0)_{kl}\\
&\quad-c_1^2H_{22}\sum_{k=1}^{N_y}\Lambda_{jl}^{y(4)}(w_0)_{il}+c_1\bar{F}_{11}\sum_{k=1}^{N_x}\Lambda_{ik}^{x(3)}(\phi_x)_{kj}+3c_1\bar{F}_{16}\sum_{k=1}^{N_x}\sum_{l=1}^{N_y}\Lambda_{ik}^{x(2)}\Lambda_{jl}^{y(1)}(\phi_x)_{kl}\\
&\quad+c_1[\bar{F}_{12}+2\bar{F}_{66}]\sum_{k=1}^{N_x}\sum_{l=1}^{N_y}\Lambda_{ik}^{x(1)}\Lambda_{jl}^{y(2)}(\phi_x)_{kl}+c_1\bar{F}_{26}\sum_{k=1}^{N_y}\Lambda_{jl}^{y(3)}(\phi_x)_{il}\\
&\quad+c_1\bar{F}_{16}\sum_{k=1}^{N_x}\Lambda_{ik}^{x(3)}(\phi_y)_{kj}+3c_1\bar{F}_{26}\sum_{k=1}^{N_x}\sum_{l=1}^{N_y}\Lambda_{ik}^{x(1)}\Lambda_{jl}^{y(2)}(\phi_y)_{kl}+c_1[\bar{F}_{12}\\
&\quad+2\bar{F}_{66}]\sum_{k=1}^{N_x}\sum_{l=1}^{N_y}\Lambda_{ik}^{x(2)}\Lambda_{jl}^{y(1)}(\phi_y)_{kl}+c_1\bar{F}_{22}\sum_{k=1}^{N_y}\Lambda_{jl}^{y(3)}(\phi_y)_{il}+\bar{\bar{A}}_{45}[\sum_{k=1}^{N_x}\Lambda_{ik}^{x(1)}(\phi_y)_{kj}\\
&\quad+\sum_{k=1}^{N_y}\Lambda_{jl}^{y(1)}(\phi_x)_{il}+2\sum_{k=1}^{N_x}\sum_{l=1}^{N_y}\Lambda_{ik}^{x(1)}\Lambda_{jl}^{y(1)}(w_0)_{kl}]+\bar{\bar{A}}_{44}[\sum_{k=1}^{N_y}\Lambda_{jl}^{y(1)}(\phi_y)_{il}\\
&\quad+\sum_{k=1}^{N_y}\Lambda_{jl}^{y(2)}(w_0)_{il}]+\bar{\bar{A}}_{55}[\sum_{k=1}^{N_x}\Lambda_{ik}^{x(1)}(\phi_x)_{kj}+\sum_{k=1}^{N_x}\Lambda_{ik}^{x(2)}(w_0)_{kj}]-N_{xx}^{T}\sum_{k=1}^{N_x}\Lambda_{ik}^{x(2)}(w_0)_{kj}\\
&\quad-2N_{xy}^{T}\sum_{k=1}^{N_x}\sum_{l=1}^{N_y}\Lambda_{ik}^{x(1)}\Lambda_{jl}^{y(1)}(w_0)_{kl}-N_{yy}^{T}\sum_{k=1}^{N_y}\Lambda_{jl}^{y(2)}(w_0)_{il}+K_p(\sum_{k=1}^{N_x}\Lambda_{ik}^{x(2)}(w_0)_{kj}\\
&\quad+\sum_{k=1}^{N_y}\Lambda_{jl}^{y(2)}(w_0)_{il})+K_w(w_0)_{ij}+q_{ij}+\omega\left[K_d(w_0)_{ij}\right]
\end{aligned}
$$

$$-\omega^2\left[m_0(w_0)_{ij}-c_1^2 m_6\left(\sum_{k=1}^{N_x}\Lambda_{ik}^{x(2)}(w_0)_{kj}+\sum_{k=1}^{N_y}\Lambda_{jl}^{y(2)}(w_0)_{il}\right)+c_1\left(m_3\left(\sum_{k=1}^{N_x}\Lambda_{ik}^{x(1)}(u_0)_{kj}+\sum_{k=1}^{N_y}\Lambda_{jl}^{y(1)}(v_0)_{il}\right)+\bar{m}_4\left(\sum_{k=1}^{N_x}\Lambda_{ik}^{x(1)}(\phi_x)_{kj}+\sum_{k=1}^{N_y}\Lambda_{jl}^{y(1)}(\phi_y)_{il}\right)\right)\right] \tag{24c}$$

$$\begin{aligned}&\bar{B}_{11}\sum_{k=1}^{N_x}\Lambda_{ik}^{x(2)}(u_0)_{kj}+2\bar{B}_{16}\sum_{k=1}^{N_x}\sum_{l=1}^{N_y}\Lambda_{ik}^{x(1)}\Lambda_{jl}^{y(1)}(u_0)_{kl}+\bar{B}_{66}\sum_{k=1}^{N_y}\Lambda_{jl}^{y(2)}(u_0)_{il}+\bar{B}_{16}\sum_{k=1}^{N_x}\Lambda_{ik}^{x(2)}(v_0)_{kj}\\&+[\bar{B}_{12}+\bar{B}_{66}]\sum_{k=1}^{N_x}\sum_{l=1}^{N_y}\Lambda_{ik}^{x(1)}\Lambda_{jl}^{y(1)}(v_0)_{kl}+\bar{B}_{26}\sum_{k=1}^{N_y}\Lambda_{jl}^{y(2)}(v_0)_{il}-c_1\bar{F}_{11}\sum_{k=1}^{N_x}\Lambda_{ik}^{x(3)}(w_0)_{kj}\\&-3c_1\bar{F}_{16}\sum_{k=1}^{N_x}\sum_{l=1}^{N_y}\Lambda_{ik}^{x(2)}\Lambda_{jl}^{y(1)}(w_0)_{kl}-c_1[\bar{F}_{12}+2\bar{F}_{66}]\sum_{k=1}^{N_x}\sum_{l=1}^{N_y}\Lambda_{ik}^{x(1)}\Lambda_{jl}^{y(2)}(w_0)_{kl}\\&-c_1\bar{F}_{26}\sum_{k=1}^{N_y}\Lambda_{jl}^{y(3)}(w_0)_{il}+\bar{\bar{D}}_{11}\sum_{k=1}^{N_x}\Lambda_{ik}^{x(2)}(\phi_x)_{kj}+2\bar{\bar{D}}_{16}\sum_{k=1}^{N_x}\sum_{l=1}^{N_y}\Lambda_{ik}^{x(1)}\Lambda_{jl}^{y(1)}(\phi_x)_{kl}\\&+\bar{\bar{D}}_{66}\sum_{k=1}^{N_x}\Lambda_{jl}^{y(2)}(\phi_x)_{il}+\bar{\bar{D}}_{16}\sum_{k=1}^{N_x}\Lambda_{ik}^{x(2)}(\phi_y)_{kj}+[\bar{\bar{D}}_{12}+\bar{\bar{D}}_{66}]\sum_{k=1}^{N_x}\sum_{l=1}^{N_y}\Lambda_{ik}^{x(1)}\Lambda_{jl}^{y(1)}(\phi_y)_{kl}\\&+\bar{\bar{D}}_{26}\sum_{k=1}^{N_y}\Lambda_{jl}^{y(2)}(\phi_y)_{il}-\bar{\bar{A}}_{45}[(\phi_y)_{ij}+\sum_{k=1}^{N_y}\Lambda_{jl}^{y(1)}(w_0)_{il}]-\bar{\bar{A}}_{55}[(\phi_x)_{ij}\\&+\sum_{k=1}^{N_x}\Lambda_{jl}^{x(1)}(w_0)_{il}]=-\omega^2\left[\bar{m}_1(u_0)_{ij}+\bar{\bar{m}}_2(\phi_x)_{ij}-c_1\bar{m}_4\sum_{k=1}^{N_x}\Lambda_{jl}^{x(1)}(w_0)_{il}\right]\end{aligned} \tag{24d}$$

$$\bar{B}_{16}\sum_{k=1}^{N_x}\Lambda_{ik}^{x(2)}(u_0)_{kj}+[\bar{B}_{12}+\bar{B}_{66}]\sum_{k=1}^{N_x}\sum_{l=1}^{N_y}\Lambda_{ik}^{x(1)}\Lambda_{jl}^{y(1)}(u_0)_{kl}+\bar{B}_{26}\sum_{k=1}^{N_y}\Lambda_{jl}^{y(2)}(u_0)_{il}$$
$$+\bar{B}_{66}\sum_{k=1}^{N_x}\Lambda_{ik}^{x(2)}(v_0)_{kj}+2\bar{B}_{26}\sum_{k=1}^{N_x}\sum_{l=1}^{N_y}\Lambda_{ik}^{x(1)}\Lambda_{jl}^{y(1)}(v_0)_{kl}+\bar{B}_{22}\sum_{k=1}^{N_y}\Lambda_{jl}^{y(2)}(v_0)_{il}$$
$$-c_1\bar{F}_{16}\sum_{k=1}^{N_x}\Lambda_{ik}^{x(3)}(w_0)_{kj}-c_1[\bar{F}_{12}+2\bar{F}_{66}]\sum_{k=1}^{N_x}\sum_{l=1}^{N_y}\Lambda_{ik}^{x(2)}\Lambda_{jl}^{y(1)}(w_0)_{kl}$$
$$-3c_1\bar{F}_{26}\sum_{k=1}^{N_x}\sum_{l=1}^{N_y}\Lambda_{ik}^{x(1)}\Lambda_{jl}^{y(2)}(w_0)_{kl}-c_1\bar{F}_{22}\sum_{k=1}^{N_y}\Lambda_{jl}^{y(3)}(w_0)_{il}+\bar{\bar{D}}_{16}\sum_{k=1}^{N_x}\Lambda_{ik}^{x(2)}(\phi_x)_{kj}$$
$$+[\bar{\bar{D}}_{12}+\bar{\bar{D}}_{66}]\sum_{k=1}^{N_x}\sum_{l=1}^{N_y}\Lambda_{ik}^{x(1)}\Lambda_{jl}^{y(1)}(\phi_x)_{kl}+\bar{\bar{D}}_{26}\sum_{k=1}^{N_y}\Lambda_{jl}^{y(2)}(\phi_x)_{il}+\bar{\bar{D}}_{66}\sum_{k=1}^{N_x}\Lambda_{ik}^{x(2)}(\phi_y)_{kj}$$
$$+2\bar{\bar{D}}_{26}\sum_{k=1}^{N_x}\sum_{l=1}^{N_y}\Lambda_{ik}^{x(1)}\Lambda_{jl}^{y(1)}(\phi_y)_{kl}+\bar{\bar{D}}_{22}\sum_{k=1}^{N_y}\Lambda_{jl}^{y(2)}(\phi_y)_{il}-\bar{\bar{A}}_{44}[(\phi_y)_{ij}$$
$$+\sum_{k=1}^{N_y}\Lambda_{jl}^{y(1)}(w_0)_{il}]-\bar{\bar{A}}_{45}[(\phi_x)_{ij}+\sum_{k=1}^{N_x}\Lambda_{jl}^{x(1)}(w_0)_{il}]$$
$$=-\omega^2\left[\bar{m}_1(v_0)_{ij}+\bar{\bar{m}}_2(\phi_y)_{ij}-c_1\bar{m}_4\sum_{k=1}^{N_x}\Lambda_{jl}^{y(1)}(w_0)_{il}\right] \tag{24e}$$

where:

$$(u_0)_{ij}=u_0(x_i,y_j),(v_0)_{ij}=v_0(x_i,y_j),(w_0)_{ij}=w_0(x_i,y_j),(\phi_x)_{ij}=\phi_x(x_i,y_j),(\phi_y)_{ij}=\phi_y(x_i,y_j)$$

Equations (24) can be rewritten as:

$$\left\{[K]+\omega[C]+\omega^2[M]\right\}\left\{\bar{W}\right\}=\{0\} \tag{25}$$

where:

$$\left\{\bar{W}\right\}=\left\{u_0 \quad v_0 \quad w_0 \quad \phi_x \quad \phi_y\right\}^T \tag{26}$$

and $[K]$, $[M]$ and $[C]$ are the equivalent stiffness, mass and damping matrices obtained by proper arranging the elements from Eqs. (24). These matrices take the form:

$$[K]=\begin{bmatrix} \mathbf{K}_{u_0u_0} & \mathbf{K}_{u_0v_0} & \mathbf{K}_{u_0w_0} & \mathbf{K}_{u_0\phi_x} & \mathbf{K}_{u_0\phi_y} \\ \mathbf{K}_{v_0u_0} & \mathbf{K}_{v_0v_0} & \mathbf{K}_{v_0w_0} & \mathbf{K}_{v_0\phi_x} & \mathbf{K}_{v_0\phi_y} \\ \mathbf{K}_{w_0u_0} & \mathbf{K}_{w_0v_0} & \mathbf{K}_{w_0w_0} & \mathbf{K}_{w_0\phi_x} & \mathbf{K}_{w_0\phi_y} \\ \mathbf{K}_{\phi_xu_0} & \mathbf{K}_{\phi_xv_0} & \mathbf{K}_{\phi_xw_0} & \mathbf{K}_{\phi_x\phi_x} & \mathbf{K}_{\phi_x\phi_y} \\ \mathbf{K}_{\phi_yu_0} & \mathbf{K}_{\phi_yv_0} & \mathbf{K}_{\phi_yw_0} & \mathbf{K}_{\phi_y\phi_x} & \mathbf{K}_{\phi_y\phi_x} \end{bmatrix}_{(5N_x\times 5N_y)} \tag{27a}$$

$$[M]=\begin{bmatrix} \mathbf{M}_{u_0u_0} & \mathbf{0} & \mathbf{M}_{u_0w_0} & \mathbf{M}_{u_0\phi_x} & \mathbf{0} \\ \mathbf{0} & \mathbf{M}_{v_0v_0} & \mathbf{M}_{v_0w_0} & \mathbf{0} & \mathbf{M}_{v_0\phi_y} \\ \mathbf{M}_{w_0u_0} & \mathbf{M}_{w_0v_0} & \mathbf{M}_{w_0w_0} & \mathbf{M}_{w_0\phi_x} & \mathbf{M}_{w_0\phi_y} \\ \mathbf{M}_{\phi_xu_0} & \mathbf{0} & \mathbf{M}_{\phi_xw_0} & \mathbf{M}_{\phi_x\phi_x} & \mathbf{0} \\ \mathbf{0} & \mathbf{M}_{\phi_yv_0} & \mathbf{M}_{\phi_yw_0} & \mathbf{0} & \mathbf{M}_{\phi_y\phi_x} \end{bmatrix}_{(5N_x\times 5N_y)} \tag{27b}$$

$$[C]=\begin{bmatrix} \mathbf{0} & \mathbf{0} & \mathbf{0} & \mathbf{0} & \mathbf{0} \\ \mathbf{0} & \mathbf{0} & \mathbf{0} & \mathbf{0} & \mathbf{0} \\ \mathbf{0} & \mathbf{0} & \mathbf{C}_{w_0w_0} & \mathbf{0} & \mathbf{0} \\ \mathbf{0} & \mathbf{0} & \mathbf{0} & \mathbf{0} & \mathbf{0} \\ \mathbf{0} & \mathbf{0} & \mathbf{0} & \mathbf{0} & \mathbf{0} \end{bmatrix}_{(5N_x\times 5N_y)} \tag{27c}$$

For eigenvalue analysis, Eq. (25) and the boundary conditions should be satisfied simultaneously. Based on GDQM, the boundary conditions can be written as constraints on the degrees of freedom as:

$$\mathbf{R}_1^{\mathrm{T}}\bar{\mathbf{W}}=\mathbf{0} \tag{28}$$

where $\mathbf{R}_1$ is matrix that depends on the type of boundary conditions. Boundary conditions involving derivatives can be defined in the form of Eq. (28) by using Eq. (18).

The boundary conditions can be enforced by defining a transformation $\mathbf{T}_1$, which is orthogonal to $\mathbf{R}_1$, i.e. $\mathbf{R}_1^{\mathrm{T}}\mathbf{T}_1=\mathbf{0}$, and where the matrix $[\mathbf{R}_1\ \mathbf{T}_1]$ is square and non-singular. One convenient option is to choose the correct number of boundary degrees of freedom (i.e. equal to the number of boundary conditions) and reorder $\bar{\mathbf{W}}$ as $\bar{\mathbf{W}}=\begin{Bmatrix}\bar{\mathbf{W}}_b\\ \bar{\mathbf{W}}_d\end{Bmatrix}$, so that $\mathbf{R}_1$ becomes

$$\mathbf{R}_1^{\mathrm{T}}=[\mathbf{R}_b\ \mathbf{R}_d] \tag{29}$$

where $\mathbf{R}_b$ is square and non-singular. A suitable transformation is then

$$\mathbf{T_1} = \begin{Bmatrix} -\mathbf{R}_b^{-1}\mathbf{R}_d \\ \mathbf{I} \end{Bmatrix}, \tag{30}$$

which eliminates the boundary degrees of freedom since

$$\bar{\mathbf{W}} = \begin{Bmatrix} \bar{\mathbf{W}}_b \\ \bar{\mathbf{W}}_d \end{Bmatrix} = \mathbf{T_1}\bar{\mathbf{W}}_d \tag{31}$$

The mass and stiffness matrices are then rearranged to match the ordering given in Eq. (29), and the transformed mass and stiffness matrices are

$$\bar{\mathbf{M}} = \mathbf{T_1^T M T_1} \quad \text{and} \quad \bar{\mathbf{C}} = \mathbf{T}^T\mathbf{C}\mathbf{T} \quad \text{and} \quad \bar{\mathbf{K}} = \mathbf{T_1^T K T_1} \tag{32}$$

The eigenvalue problem then becomes

$$[\bar{\mathbf{K}} + \omega\bar{\mathbf{C}} + \omega^2\bar{\mathbf{M}}]\bar{\mathbf{W}}_d = \mathbf{0} \tag{33}$$

The standard form for the solution of the eigenvalue problem in Eq. (33) is:

$$\begin{bmatrix} -\bar{\mathbf{M}}^{-1}\mathbf{C} & -\bar{\mathbf{M}}^{-1}\mathbf{K} \\ \mathbf{I} & \mathbf{0} \end{bmatrix} \begin{Bmatrix} \dot{\bar{\boldsymbol{W}}}_d \\ \bar{\mathbf{W}}_d \end{Bmatrix} = \omega \begin{Bmatrix} \dot{\bar{\boldsymbol{W}}}_d \\ \bar{\mathbf{W}}_d \end{Bmatrix} \tag{34}$$

The eigenvalues of Eq. (34) are complex, where the real part describes the damping characteristics and the imaginary part gives the damped natural frequency.

4. Numerical Results and Discussions

In this section, the numerical results are of the vibration analysis aare obtained for anti-symmetric laminated composite plates considering the variation of eight parameters. The effects of temperature, Winkler coefficient, Pasternak coefficient, elastic ratio, different anti-symmetric laminates arrangement, aspect and slenderness ratios are illustrated and discussed in detail. The results in Sections 4.1 to 4.8 are extracted for CCCC boundary conditions with $k_d = 0$. Also, the effects of other boundary conditions and the visco-damping coefficient are given in Sections 4.9 and 4.10 respectively. For the parameter studies, we fix six of the parameters out of the eight parameters available at each step and change the remaining two parameters to investigate the effects and their interactions. The thermo-mechanical properties of carbon/epoxy lamina which is utilized for the simulation are given in Table 1:

Table 1: Material properties of carbon/epoxy composite [13]

$E_1\,(GPa)$	$E_2\,(GPa)$	$G_{12}=G_{13}=G_{23}\,(GPa)$	ν_{12}
140	10	7	0.3
$\alpha_1\,(^{\circ}C^{-1})$	$\alpha_2\,(^{\circ}C^{-1})$	$\rho\,(kg/m^3)$	$h\,(mm)$

1e-6	30e-6	1520	25

4.1. DQM Accuracy and convergency

Fig. 2 shows the effect of the number of grid points on the caculated natural frequency and evaluates the accuracy and convergence of the DQM. The fast rate of convergence of the DQM is easily observed. Accurate results can be obtained for grids with $N_x = N_y = 19$ points for $\lambda = 1$ and $N_x = N_y = 25$ points for $\lambda = 4$. Hence the aspect ratio affects the convergence rate of the DQM, and thus to ensure sufficient accuracy in the following results the number of grid points is set to $N_x = N_y = 27$. Accuracy, fast convergence and simplicity are the advantages of the DQM compared to other numerical methods such as the finite element method, the finite difference method and the boundary element method.

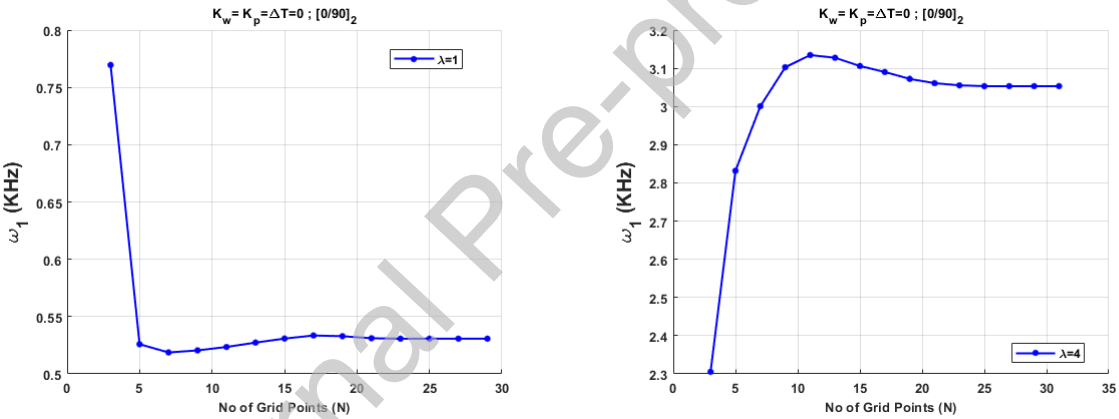

Fig. 2: Convergence and accuracy of the DQM for a $[0/90]_2$ laminated plate. Here $N = N_x = N_y$.
a) aspect ratio=1 b) aspect ratio=4

4.2. Comparison of First and Higher Order Shear Deformation Theories

In this section the results are compared for first shear deformation theory (FSDT) and higher-order shear deformation theory (HSDT). Although CLP and FSD theories can easily describe the kinematics of most plates and are not complicated, the higher-order shear deformation theories (HSDT) estimate the kinematics more accurately. This results in more accurate inter-laminar stress distributions and it is not necessary to apply shear correction factors. Moreover, higher-order shear deformation theories can describe the behavior of thick plates more accurately. Fig. 3 shows the

difference between FSDT and HSDT for two different aspect ratios, $\lambda = 1, 2$. Figs. 3(a) and 3(b) show the variation with respect to the slenderness ratio, L_x/h, and Figs. 3(c) and 3(d) show the variation with respect to the elastic ratio E_1/E_2. According to these results, for thick plates or low values of slenderness ratio, where the plates have high values of the elastic ratio and a high aspect ratio, the deviation between FSDT and HSDT is obvious.

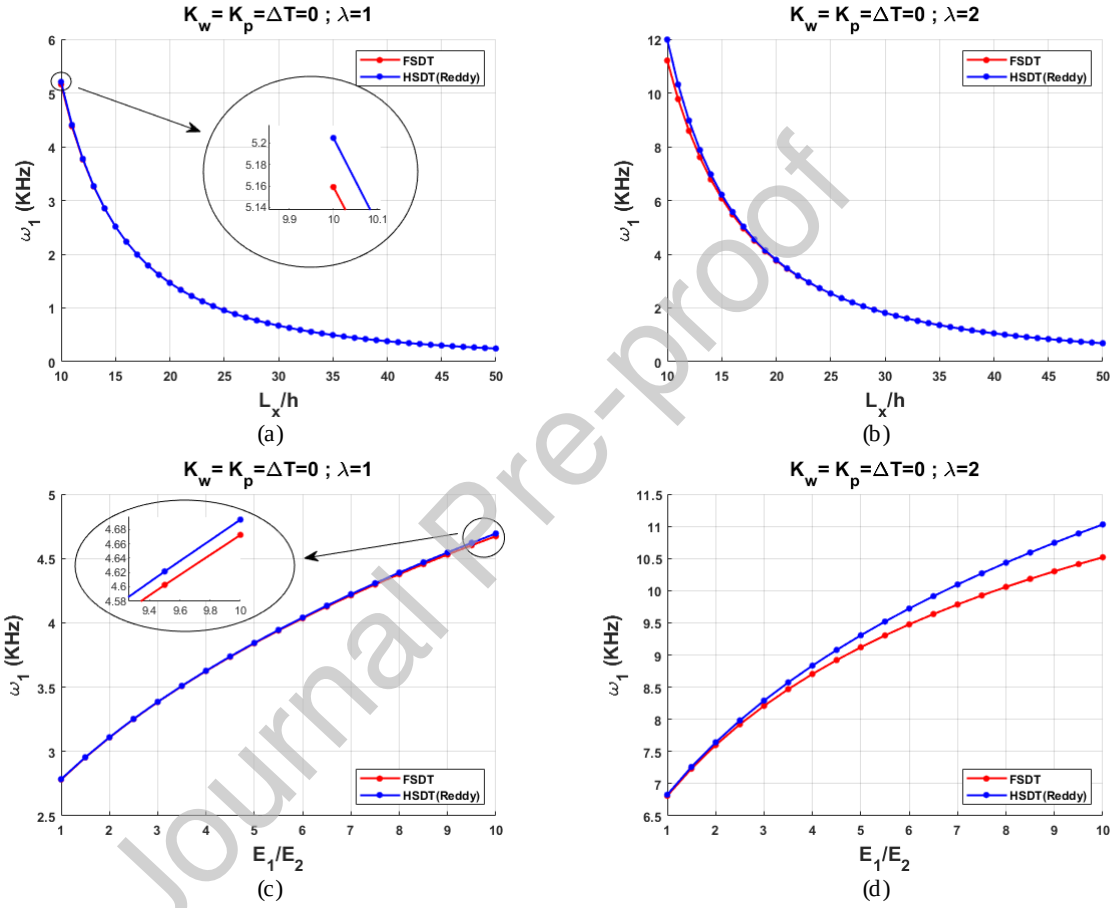

Fig. 3: Comparison between FSDT and HSDT based on the variation of slenderness and elastic ratios for $[0/90]_2$
a) different slenderness ratio and aspect ratio=1 b) different slenderness ratio and aspect ratio=2
c) different elastic ratio and aspect ratio=1 d) different elastic ratio and aspect ratio=2

4.3. Model Validation

To validate the current model and verify the accuracy of the obtained results, the numerical results from the proposed model for the fundamental non-dimensional frequency, $\bar{\omega}_1$, with the materials of Ref. [65] are compared to the numerical results of Ref. [65], which were obtained by the Ritz method. The results are shown in Table 2 and are obtained for [45/45], [0/90], [45/-45] and [0/45]

layups, and fully-clamped and fully-simply-supported boundary conditions. Based on the DQM accuracy and convergence analysis presented in Section 4.1, the fundamental natural frequency estimates are sufficiently accurate for *N*=25 grid points, and *N*=27 grid points are used in our simulations. However, here *N*=33 grid points are used so that the presented results are more accurate than the results of Ref. [65]. Also, the DQM has two main advantages compared with the Ritz method, which are not very accurate for curved shells and cannot consider damped structures.

Table 2: Model validation of a square plate by comparing the fundamental non-dimensional natural frequency $\bar{\omega}_1 = \omega_1 (L_x^2 / h)\sqrt{\rho / E_2}$

		$L_x/h=5$		$L_x/h=100$	
		Ref. [65]	Proposed	Ref. [65]	Proposed
SSSS	[45/45]	18.1320	18.1215	22.0812	22.0702
	[0/90]	13.4136	13.4021	14.4961	14.4876
	[45/-45]	19.0494	19.0401	23.8015	23.7851
	[0/45]	15.1286	15.1191	17.2967	17.2901
CCCC	[45/45]	24.2226	24.2096	40.3987	40.3807
	[0/90]	23.7414	23.7303	30.8179	30.8100
	[45/-45]	22.8171	22.7998	29.9020	29.8123
	[0/45]	23.1717	23.1617	31.3885	31.3771

The comparison of the results in Table 2 shows good agreement between the results of the proposed method and the results of Ref. [65], which verifies our model.

4.4. Effects of Laminates Arrangement

The effect of the arrangement of the laminates on the fundamental frequency is illustrated in Figs 4 and 5. The results are observed based on the variation of the aspect ratio $\lambda = L_x / L_y$ from 0.5 to 4 for different symmetric and anti-symmetric laminate arrangements. Fig. 4 shows the fundamental frequency variations based on the four types of different anti-symmetric layups of the composite plate, namely $(0/90)_n$, $(45/-45)_n$, $(30/-30)_n$ and $(5/-5)_n$ for $n = 1, 2, 3$. For all cases, the natural frequencies increase with the increase in the aspect ratio and also increase with the number of anti-symmetric layers. However, the arrangement of the layups has a contradictory effect on the natural frequency. That is, for low aspect ratios, the frequency for $(5/-5)_n$ is higher than the other layups and after a certain aspect ratio, the effect of the laminate arrangement will be reverse. For example, in Fig. 4(b), up to $\lambda = 1$ the frequency for $(5/-5)_2$ is higher and for $\lambda > 1$

the frequency of $(5/-5)_2$ is lower than the other layups. So, for this condition $\lambda = 1$ is called the intersection point. Moreover, it is obvious as the number of anti-symmetric layers increases the mentioned contradictory effect will appear for low λ values.

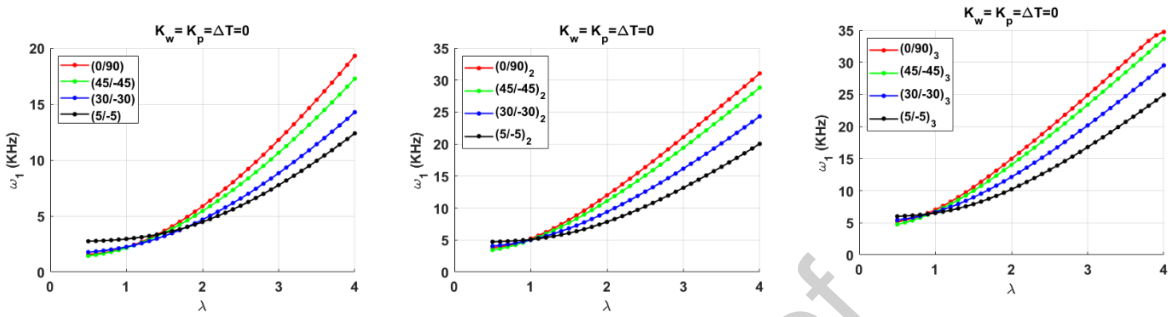

Fig. 4: Fundamental frequency based on the variation of aspect ratio and different laminates arrangement

Fig. 5 compares the effect of the symmetric and anti-symmetric laminates arrangement on the fundamental natural frequency. The results are illustrated for symmetric and anti-symmetric laminates arrangement of $(0/\theta)_2$ and $(0/\theta/0/\theta)_2$ for $\theta = 5, 30, 45, 90^\circ$. With increasing θ, the difference of the symmetric and anti-symmetric laminates arrangement effect on the fundamental frequency is more evident. As an example, when $\theta = 5^\circ$, the symmetric and anti-symmetric arrangement of the laminates has no significant effect on the fundamental frequency. However, there is a considerable difference between the symmetric and anti-symmetric arrangement of the laminates for $\theta = 90^\circ$.

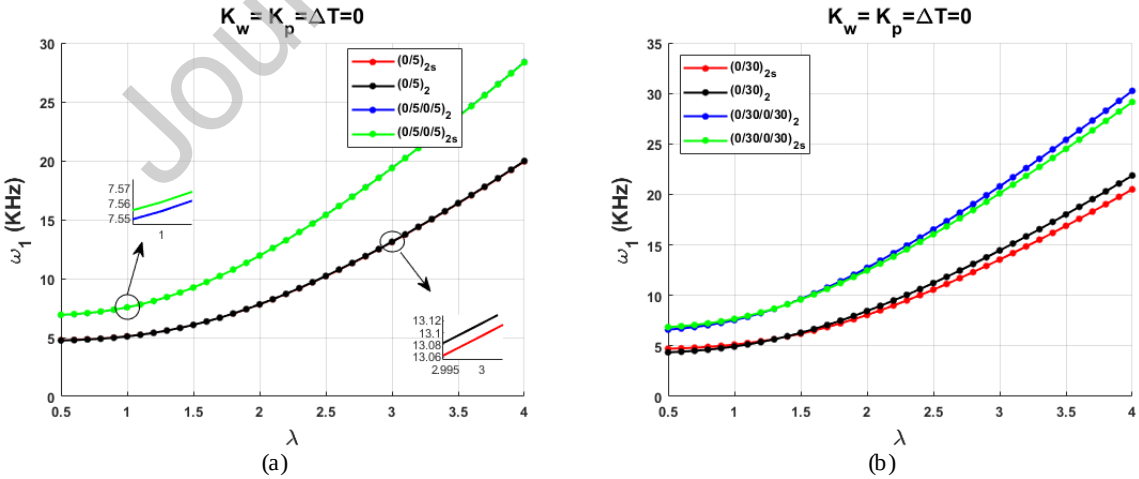

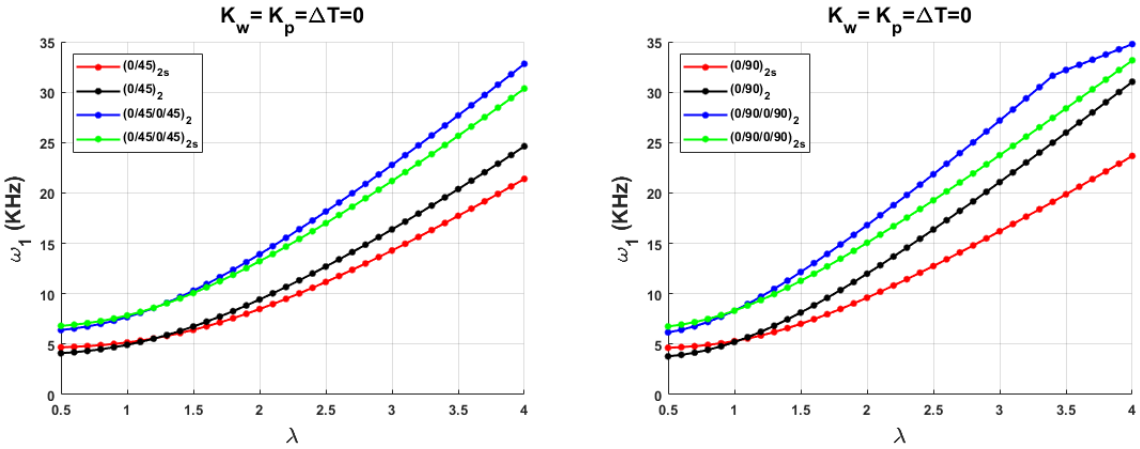

Fig. 5: Comparison of the symmetric and anti-symmetric laminates arrangement on the fundamental frequency

In addition, up to a certain value of λ, the fundamental frequency for symmetric laminates is higher than for the anti-symmetric laminates but, for higher values of λ this changes and the fundamental frequency for anti-symmetric laminates will be higher.

4.5. Effects of Elastic Ratio

In this section, the effects of elastic ratio E_1/E_2 on the fundamental frequency is considered. To extract the results, we fix the value of E_2 and change the value of E_1 to achieve the ratio from 10 to 70. Also, the results are obtained for symmetric and anti-symmetric laminates arrangement with $(0/\theta)_2$ and $(0/\theta/0/\theta)_2$ for $\theta = 5, 30, 45, 90^\circ$. Fig. 6 shows that the fundamental frequency increases with as the elastic ratio increases due to the increasing stiffness of the composite plate. Also, the effects of the symmetric and anti-symmetric laminates arrangement along with the effects of the elastic ratio on the fundamental frequency can be tracked simultaneously in Fig. 6. As an example, in Figs. 6(a) and 6(b) the results are plotted for the anti-symmetric $(0/\theta)_2$ layup with $\lambda = 1$ and 0.5 respectively. It can be easily seen that when $\lambda = 0.5$ the fundamental frequency for $(0/5)_2$ is the highest and for $(0/90)_2$ is the lowest. But, for $\lambda = 1$ in Fig. 6(a), and due to the proximity to the intersection point, the fundamental frequencies for the layups will be different.

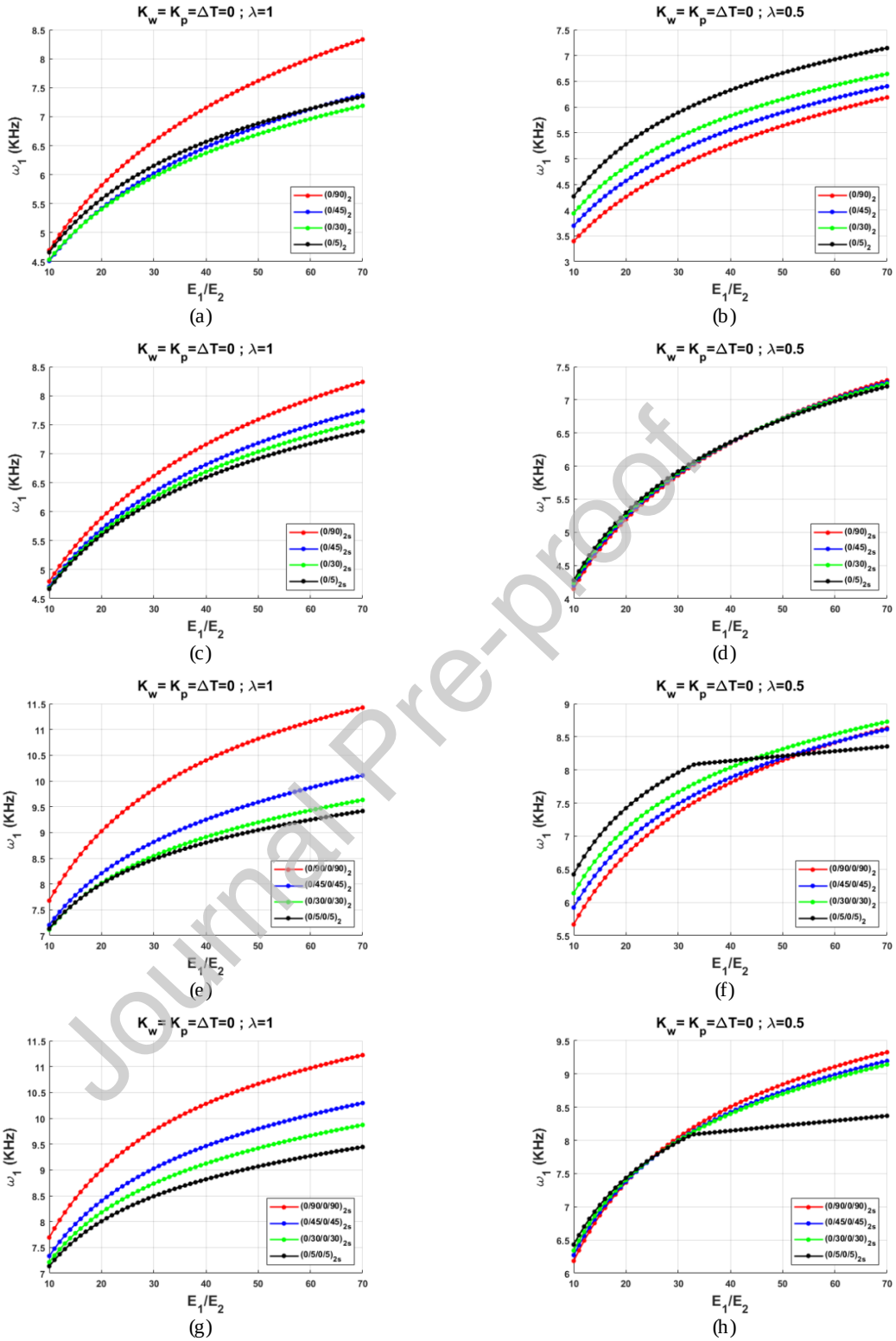

Fig. 6: Effects of the elastic ratio of the symmetric and anti-symmetric laminates arrangement on the fundamental frequency

4.6. Effects of the Winkler Coefficient

The effects of the Winkler coefficient on the fundamental frequency are illustrated based on the variation of the aspect ratio λ, and the slenderness ratio L_x/h, in Figs. 7 and 8 respectively. The results are obtained for the variation of the Winkler coefficient k_w, from 0 to 3 GN/m^3 in six steps. Also, the anti-symmetric layups $(0/90)_n$, $(45/-45)_n$, $(30/-30)_n$ and $(5/-5)_n$ for $n=1,2,3$ are considered to establish the results.

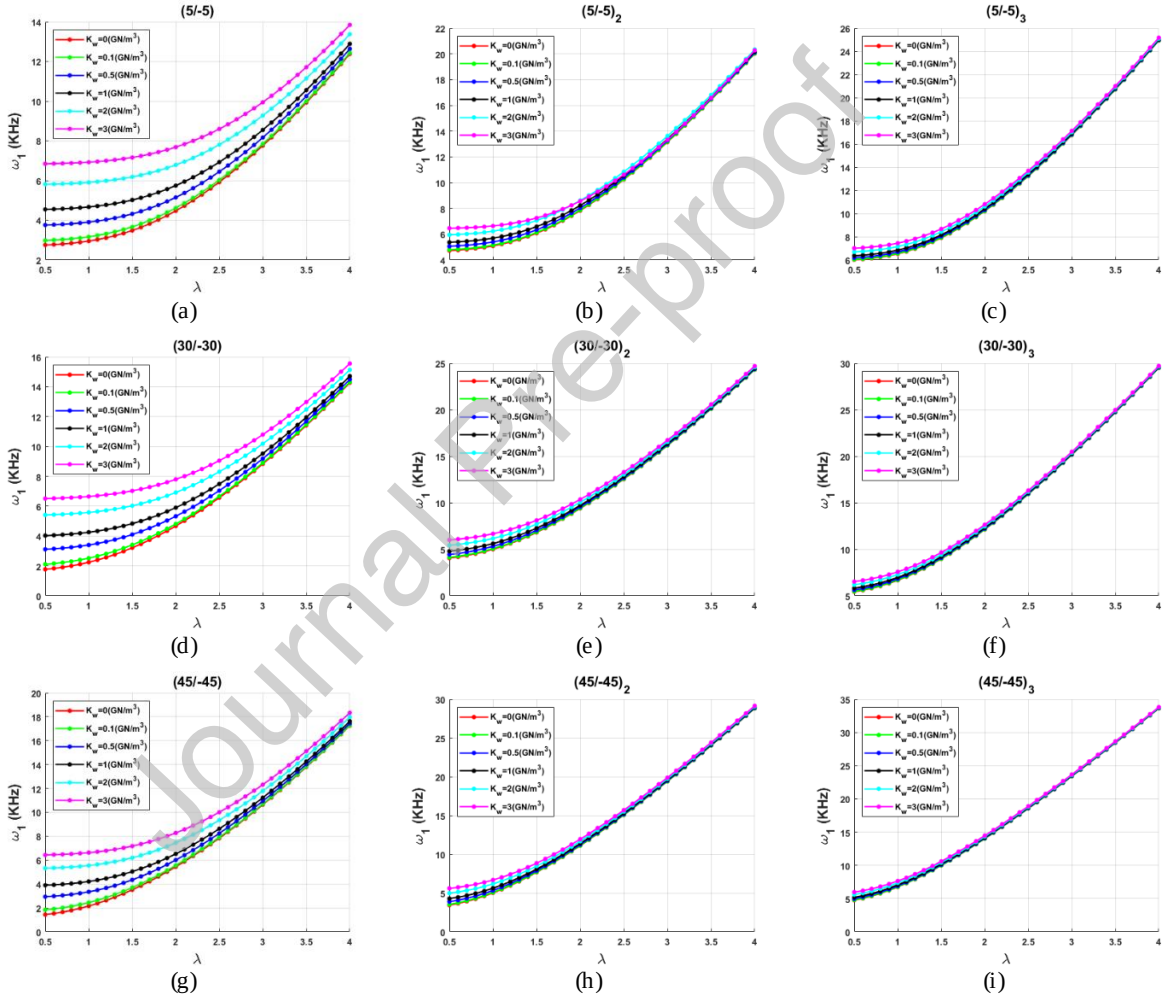

(a) (b) (c)

(d) (e) (f)

(g) (h) (i)

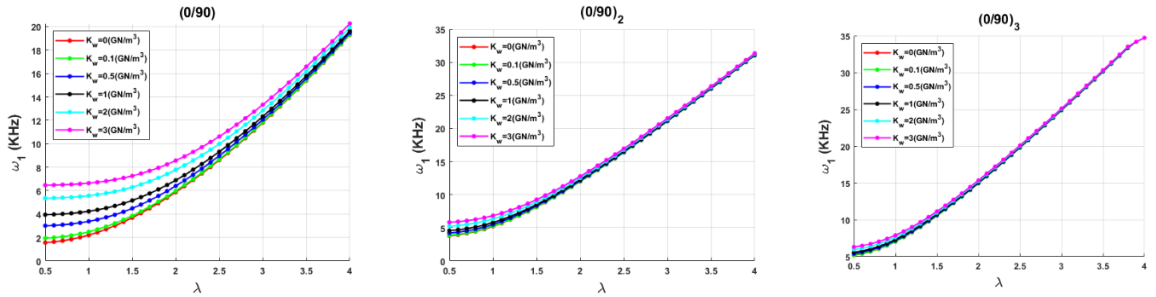

(k) (l) (m)

Fig. 7: Effects of the Winkler coefficient on the fundamental frequency as the aspect ratio varies

According to Fig. 7, for all cases, increasing the Winkler coefficient leads to an increase in the fundamental frequency. However, with increasing the aspect ratio, the variation of the Winkler coefficient has no significant effect on the fundamental frequency. Furthermore, as the number of the anti-symmetric laminates increases the variation of the Winkler coefficient also has no significant effect on the fundamental frequency.

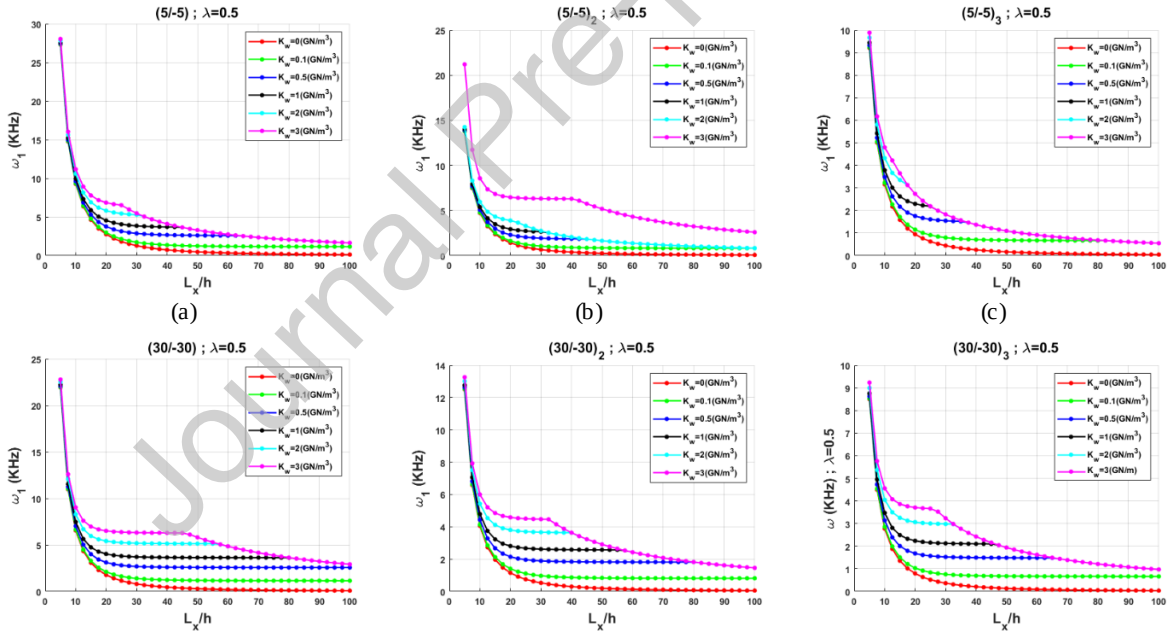

(a) (b) (c)

(d) (e) (f)

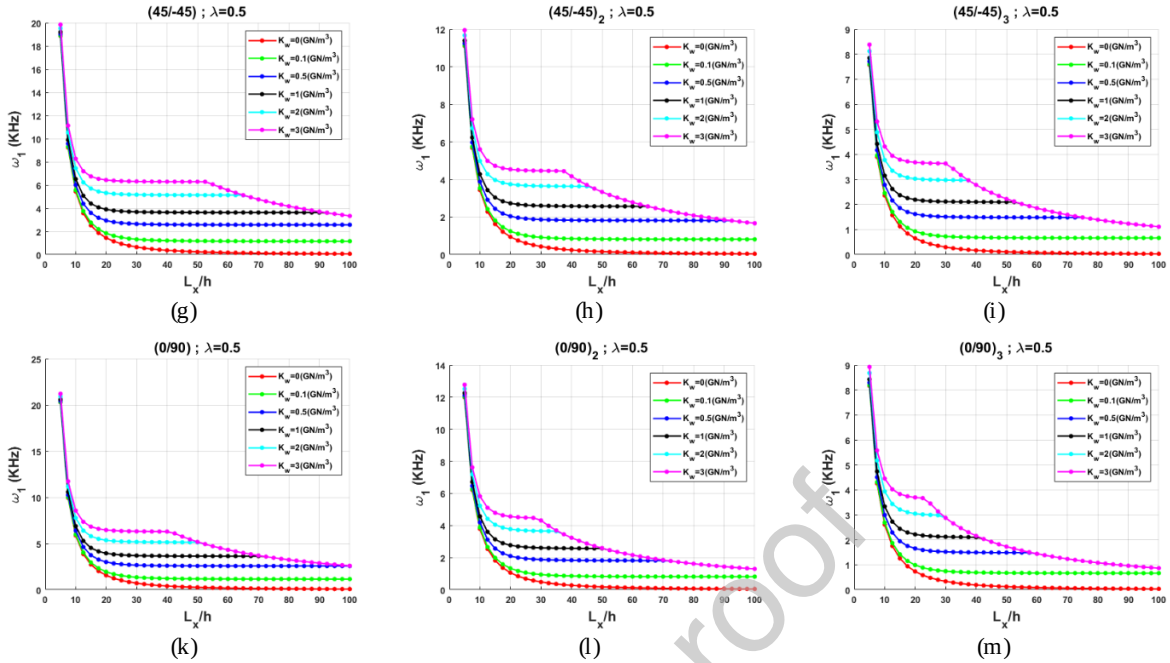

Fig. 8: Effects of the Winkler coefficient on the fundamental frequency as the slenderness ratio varies

Fig. 8 shows the effects of the Winkler coefficient on the fundamental frequency as the slenderness ratio varies. As the slenderness ratio increases the fundamental frequency decreases. Also, after a certain value of the slenderness ratio the variation of the Winkler coefficient has no effect on the fundamental frequency.

4.7. Effects of Pasternak Coefficient

The effects of the Pasternak coefficient on the fundamental frequency is observed in Fig. 9 for different aspect ratios from 0.5 to 4 in six steps. The Pasternak coefficient is changed from 0 to 1 GN/m and anti-symmetric layups $(0/90)_n$, $(45/-45)_n$, $(30/-30)_n$ and $(5/-5)_n$ for $n=1,2,3$ are considered.

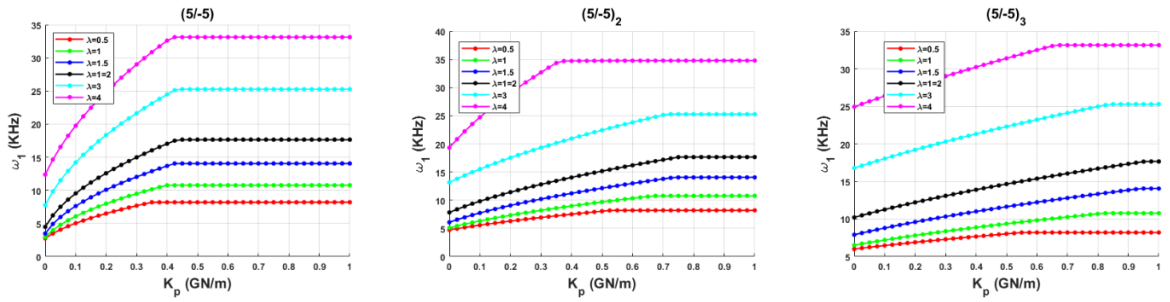

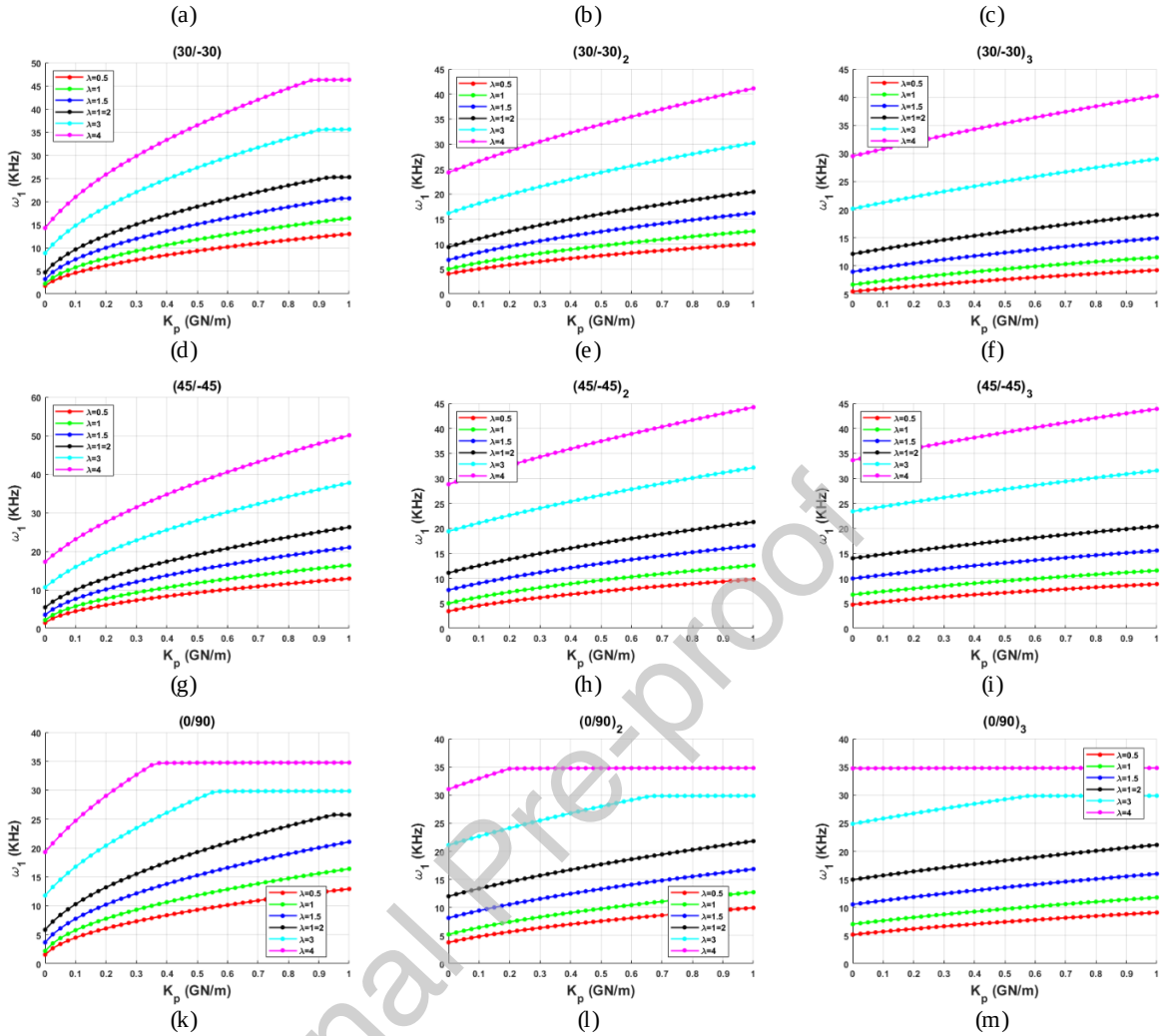

Fig. 9: Effects of the Pasternak coefficient on the fundamental frequency for different aspect ratios

On the basis of the results, the fundamental frequency increases up to a certain value with increasing Pasternak coefficient. In other words, the increase of the Pasternak coefficient up to a specific value, called the corner point, affects the fundamental frequency and for coefficients higher than the corner point there is no effect on the frequency. As an example, in Fig. 9(k) for $\lambda = 4$, $\lambda = 3$ and $\lambda = 2$, the corner points are at $k_p = 0.37$, $k_p = 0.56$ and $k_p = 0.95$ respectively. For other aspect ratios, the corner points will definitely occur for $k_p > 1$, which are not displayed in the figure. Moreover, the arrangement of the layups and the number of the anti-symmetric layers affect the corner points. For example, according to Figs. 9(a) to 9(c) and for

$\lambda = 2$, the corner points are located at $k_p = 0.43$, $k_p = 0.7$ and $k_p = 0.85$ for the anti-symmetric layups $(5/-5)$, $(5/-5)_2$ and $(5/-5)_3$ respectively. Note that these values can differ for the same layups with different aspect ratios, and for other layups can be different.

4.8. Effects of Temperature

Fig. 10 shows the variation of the fundamental frequency as the temperature varies for different anti-symmetric laminate arrangements with $(0/90)_n$, $(45/-45)_n$, $(30/-30)_n$ and $(5/-5)_n$ layups when $n = 1,2,3$ and for three different aspect ratios, $\lambda = 1.5,2,3$. In this section, based on aerospace applications, the temperature variation is considered from -60 to $140\,^{\circ}C$.

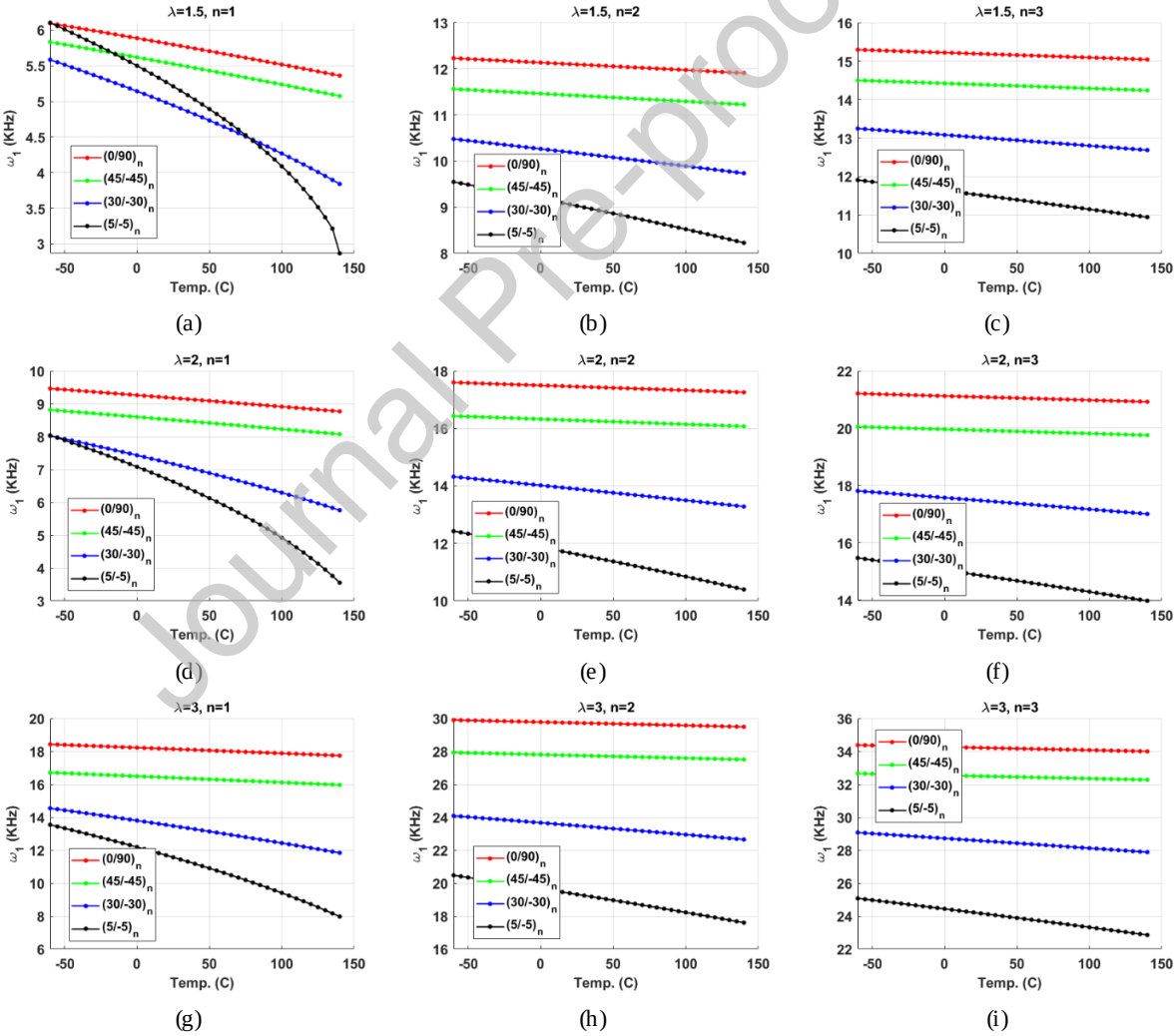

Fig. 10: Effects of the temperature on the fundamental frequency for different aspect ratios and different layups

Fig. 10 shows that as the aspect ratio and the number of anti-symmetric layers increase, the decreasing gradient of the fundamental frequency will be smoother. In addition, the decreasing gradient of the fundamental frequency for $(5/-5)_n$ layups is sharper and for $(0/90)_n$ is smoother than the others.

4.9. Effects of Boundary Conditions

Fig. 11 shows the results for different boundary conditions. The results are reported for fully-clamped (CCCC), fully- simply supported (SSSS) and the combination of these two types of boundary conditions, as the slenderness ratio varies. The results are presented for two different anti-symmetric layups of $(0/90)_2$ and $(0/90/0/90)_2$ with $\lambda = 3$. The fundamental frequency of the plate is highest for CCCC and lowest for SSSS boundary conditions. The effects of the other boundary conditions on the fundamental frequency are also illustrated in Fig. 11.

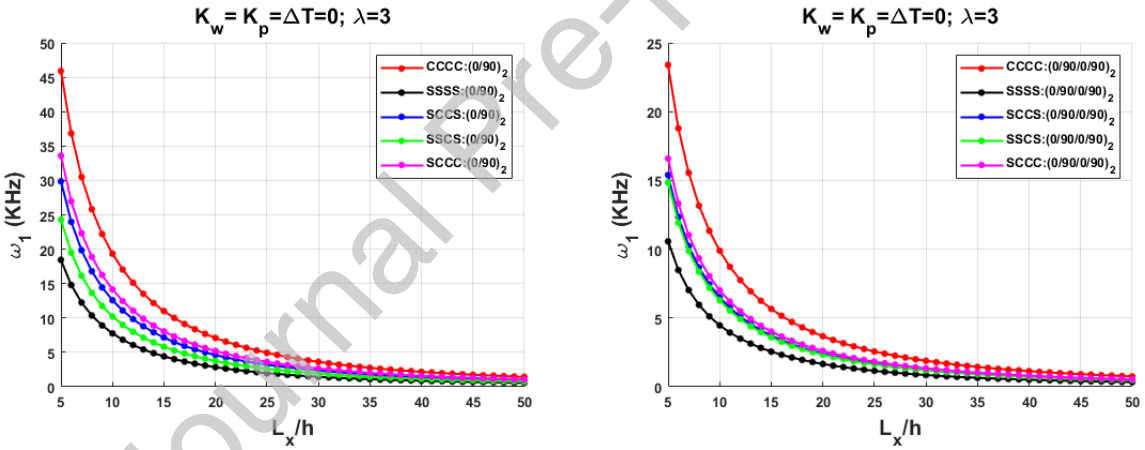

Fig. 11: Effects of the boundary conditions on the fundamental frequency for different slenderness ratios

4.10. Effects of the Visco-elastic Damping Coefficient

The effects of viscoelastic damping on the fundamental damped frequency are now illustrated. The variation of the damping ratio is investigated as the viscoelastic parameter varies. Figure 12 shows the fundamental damped natural frequency and the damping ratio versus the parameter k_d for different layup arrangements. The results are obtained for anti-symmetric laminates arrangements

of $(-\theta/\theta)_2$ and $(-\theta/\theta/-\theta/\theta)_2$ for $\theta = 5, 30, 45^\circ$, and also for laminates $(0/90)_2$ and $(0/90/0/90)_2$. The value of k_d is changed from 0 to 10 and considered on a logarithmic scale. The fundamental damped natural frequency, ω_{1d}, decreases as k_d increases. However, the trend of the damping ratio is the reverse and increases with increasing k_d.

Also, the simultaneous effect of the aspect ratio λ and the viscoelastic coefficient k_d, on the damping ratio for different layups is given in Fig. 13. Based on the results, as the aspect ratio increases, the slope of the damping ratio reduces. As the number of layers increases, the damping ratio is lower for the same value of viscoelastic coefficient k_d.

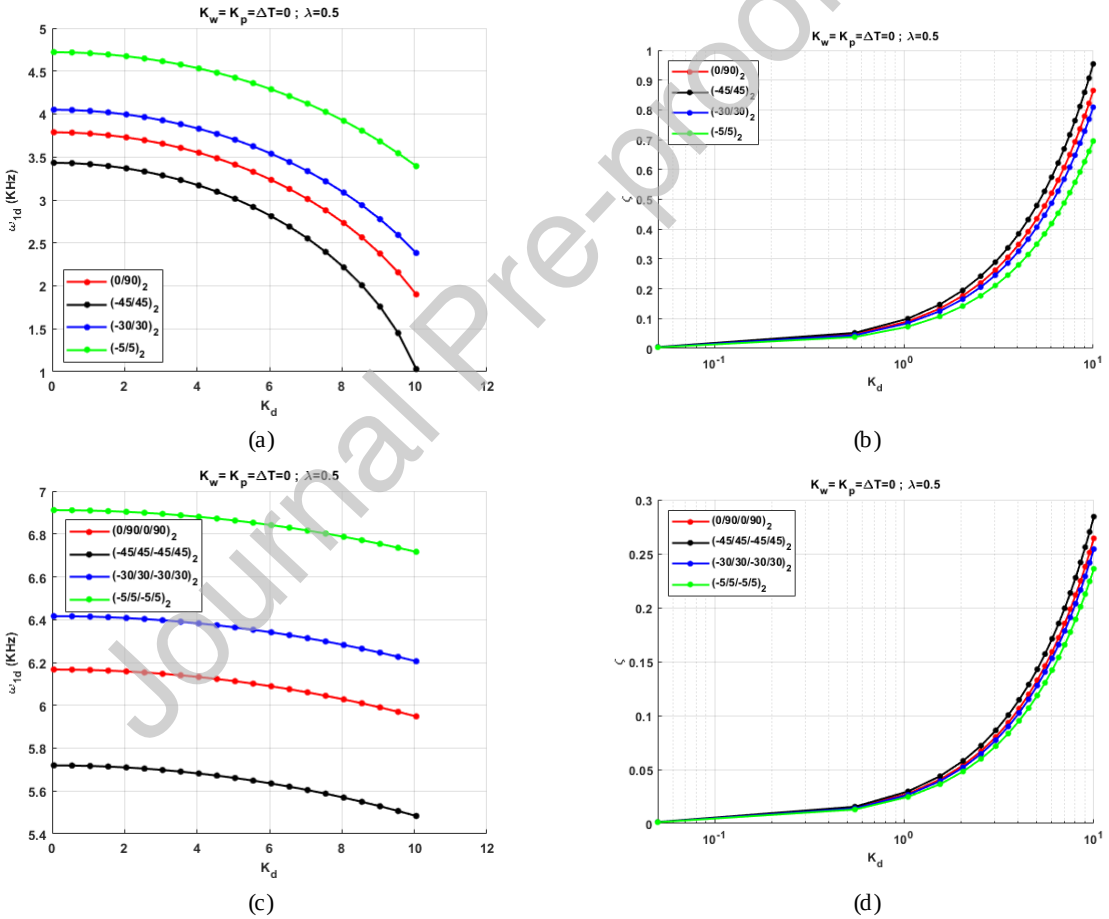

Fig. 12: Effects of the visco-elastic coefficient on the fundamental damped frequency and damping ratio of laminated plates
a) and b) Anti-symmetric layups $(-\theta/\theta)_2$
c) and d) Anti-symmetric layups $(-\theta/\theta/-\theta/\theta)_2$

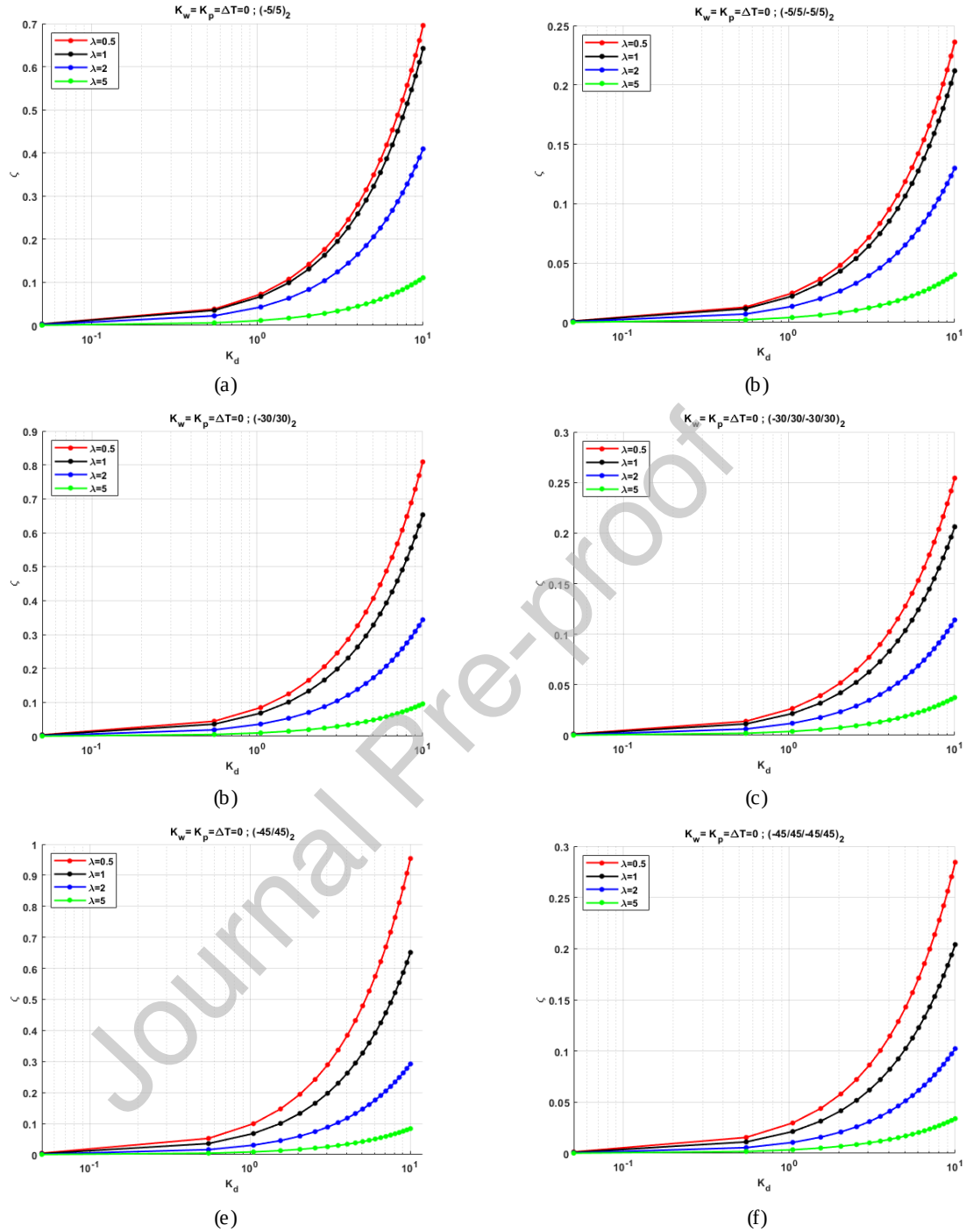

Fig. 13: Effects of the visco-elastic coefficient on the damping ratio of laminated plates for different anti-symmetric layups

5. Conclusions

The goal of this paper is to present a comprehensive mathematical-mechanical model to investigate oscillations of an anti-symmetric composite plate resting on a visco-elastic foundation incorporating thermal effects. A higher-order shear deformation plate theory is employed to develop the equations of motion and GDQM is utilized to solve the governing equations. Also, the effects of temperature change, Winkler-Pasternak and damping coefficients for elastic foundation, the elastic ratio, different anti-symmetric laminates arrangement, and the aspect and slenderness ratios are observed and discussed in detail. Important and notable findings are summarized as:

1. The fundamental frequencies increase as the number of anti-symmetric layers increases.
2. The arrangement of the layups has a contradictory effect on the frequency.
3. The fundamental frequency increases as the elastic ratio increases.
4. Increasing the Winkler coefficient increases the fundamental natural frequency and with increasing aspect ratio, the variation of the Winkler coefficient has no significant effect on the fundamental frequency.
5. The fundamental frequency increases up to a certain value with increasing Pasternak coefficient. Also, increasing the Pasternak coefficient up to a specific value, called the corner point, affects the fundamental frequency, whereas values higher than the corner point have no effect on the frequency.
6. The frequency generally decreases as the temperature increases.
7. The fundamental frequency of the plate was obtained for different boundary conditions.
8. Increasing the viscoelastic coefficient, decreases the natural frequency and increases the damping ratio.

Nonlinear vibration analysis, a visco-elastic composite model and nonlinear temperature fields are topics for future research.

References

[1] Kassapoglou C. Design and analysis of composite structures: with applications to aerospace structures: John Wiley & Sons, 2013.

[2] Beardmore P. Composite structures for automobiles. Composite Structures. 1986;5:163-76.

[3] Hollaway LC. Advanced polymer composites and polymers in the civil infrastructure: Elsevier, 2001.

[4] Bhavya S, Velmurugan R, Arunachalam K. Evaluation of E glass epoxy composite laminate as an electromagnetically transparent aerospace material. Materials Today: Proceedings. 2020.

[5] Huang Y, Zhang Z, Li C, Wang J, Li Z, Mao K. Sound Radiation of Orthogonal Antisymmetric Composite Laminates Embedded with Pre-Strained SMA Wires in Thermal Environment. Materials. 2020;13:3657.

[6] Joshan YS, Santapuri S, Grover N. Analysis of laminated piezoelectric composite plates using an inverse hyperbolic coupled plate theory. Applied Mathematical Modelling. 2020;82:359-78.

[7] Li C, Han Q, Wang Z, Wu X. Analysis of wave propagation in functionally graded piezoelectric composite plates reinforced with graphene platelets. Applied Mathematical Modelling. 2020;81:487-505.

[8] Qin X, Dong C, Yang H. Isogeometric vibration and buckling analyses of curvilinearly stiffened composite laminates. Applied Mathematical Modelling. 2019;73:72-94.

[9] Liu C, Yu J, Zhang B, Zhang X. Reflection and transmission of elastic waves in the multilayered orthotropic couple-stressed plates sandwiched between two elastic half-spaces. Applied Mathematical Modelling. 2019;75:52-72.

[10] Naghsh A, Azhari M, Saadatpour M. Thermal buckling analysis of point-supported laminated composite plates in unilateral contact. Applied Mathematical Modelling. 2018;56:564-83.

[11] Zhang Z, Wu H, Ye G, Wu H, He X, Chai G. Systematic experimental and numerical study of bistable snap processes for anti-symmetric cylindrical shells. Composite Structures. 2014;112:368-77.

[12] Li D. Layerwise Theories of Laminated Composite Structures and Their Applications: A Review. Archives of Computational Methods in Engineering. 2020:1-24.

[13] Reddy JN. Mechanics of laminated composite plates and shells: theory and analysis: CRC press, 2003.

[14] Sayyad AS, Ghugal YM. Static and free vibration analysis of laminated composite and sandwich spherical shells using a generalized higher-order shell theory. Composite Structures. 2019;219:129-46.

[15] Malekzadeh P, Afsari A, Zahedinejad P, Bahadori R. Three-dimensional layerwise-finite element free vibration analysis of thick laminated annular plates on elastic foundation. Applied Mathematical Modelling. 2010;34:776-90.

[16] Zhao J, Choe K, Shuai C, Wang A, Wang Q. Free vibration analysis of laminated composite elliptic cylinders with general boundary conditions. Composites Part B: Engineering. 2019;158:55-66.

[17] Antunes AM, Ribeiro P, Rodrigues JD, Akhavan H. Modal analysis of a Variable Stiffness Composite Laminated plate with diverse boundary conditions: Experiments and modelling. Composite Structures. 2020;239:111974.

[18] Quintana MV, Raffo JL. A variational approach to vibrations of laminated composite plates with a line hinge. European Journal of Mechanics-A/Solids. 2019;73:11-21.

[19] Wang Q, Shao D, Qin B. A simple first-order shear deformation shell theory for vibration analysis of composite laminated open cylindrical shells with general boundary conditions. Composite Structures. 2018;184:211-32.

[20] Malekzadeh P, Zarei A. Free vibration of quadrilateral laminated plates with carbon nanotube reinforced composite layers. Thin-Walled Structures. 2014;82:221-32.

[21] Maji A, Mahato PK. Development and applications of shear deformation theories for laminated composite plates: An overview. Journal of Thermoplastic Composite Materials. 2020:0892705720930765.

[22] Thai H-T, Kim S-E. Free vibration of laminated composite plates using two variable refined plate theory. International Journal of Mechanical Sciences. 2010;52:626-33.

[23] Zhu P, Lei Z, Liew KM. Static and free vibration analyses of carbon nanotube-reinforced composite plates using finite element method with first order shear deformation plate theory. Composite Structures. 2012;94:1450-60.

[24] Mantari J, Oktem A, Soares CG. A new higher order shear deformation theory for sandwich and composite laminated plates. Composites Part B: Engineering. 2012;43:1489-99.

[25] Fazzolari FA, Carrera E. Accurate free vibration analysis of thermo-mechanically pre/post-buckled anisotropic multilayered plates based on a refined hierarchical trigonometric Ritz formulation. Composite Structures. 2013;95:381-402.

[26] Fazzolari FA, Carrera E. Free vibration analysis of sandwich plates with anisotropic face sheets in thermal environment by using the hierarchical trigonometric Ritz formulation. Composites Part B: Engineering. 2013;50:67-81.

[27] Chen C-S, Chen C-W, Chen W-R, Chang Y-C. Thermally induced vibration and stability of laminated composite plates with temperature-dependent properties. Meccanica. 2013;48:2311-23.

[28] Nedri K, El Meiche N, Tounsi A. Free vibration analysis of laminated composite plates resting on elastic foundations by using a refined hyperbolic shear deformation theory. Mechanics of Composite Materials. 2014;49:629-40.

[29] Li X, Yu K, Han J, Song H, Zhao R. Buckling and vibro-acoustic response of the clamped composite laminated plate in thermal environment. International Journal of Mechanical Sciences. 2016;119:370-82.

[30] Kiani Y. Free vibration of FG-CNT reinforced composite skew plates. Aerospace Science and Technology. 2016;58:178-88.

[31] Pingulkar P, Suresha B. Free Vibration Analysis of Laminated Composite Plates Using Finite Element Method. Polymers and Polymer Composites. 2016;24:529-38.

[32] Zhang H, Shi D, Wang Q. An improved Fourier series solution for free vibration analysis of the moderately thick laminated composite rectangular plate with non-uniform boundary conditions. International Journal of Mechanical Sciences. 2017;121:1-20.

[33] Zamani H, Aghdam M, Sadighi M. Free vibration analysis of thick viscoelastic composite plates on visco-Pasternak foundation using higher-order theory. Composite Structures. 2017;182:25-35.

[34] Zhang L, Selim B. Vibration analysis of CNT-reinforced thick laminated composite plates *based on Reddy's higher*-order shear deformation theory. Composite Structures. 2017;160:689-705.

[35] Canales F, Mantari J. Free vibration of thick isotropic and laminated beams with arbitrary boundary conditions via unified formulation and Ritz method. Applied Mathematical Modelling. 2018;61:693-708.

[36] Chernikov D, Zhupanska OI, Krokhmal P. Optimization of dynamic mechanical response of a composite plate using multi-field coupling with thermal constraints. Applied Mathematical Modelling. 2018;58:19-32.

[37] Fallah N, Delzendeh M. Free vibration analysis of laminated composite plates using meshless finite volume method. Engineering Analysis with Boundary Elements. 2018;88:132-44.

[38] Alaimo A, Orlando C, Valvano S. Analytical frequency response solution for composite plates embedding viscoelastic layers. Aerospace Science and Technology. 2019;92:429-45.

[39] Zhang S, Xu L, Li R. New exact series solutions for transverse vibration of rotationally-restrained orthotropic plates. Applied Mathematical Modelling. 2019;65:348-60.

[40] Hachemi M, Hamza-Cherif S. Free vibration of composite laminated plate with complicated cutout. Mechanics Based Design of Structures and Machines. 2019:1-25.

[41] Tanzadeh H, Amoushahi H. Buckling and free vibration analysis of piezoelectric laminated composite plates using various plate deformation theories. European Journal of Mechanics-A/Solids. 2019;74:242-56.

[42] Vidal P, Gallimard L, Polit O. Free vibration analysis of composite plates based on a variable separation method. Composite Structures. 2019;230:111493.

[43] Faroughi S, Shafei E, Rabczuk T. Anisotropic solid-like shells modeled with NURBS-based isogeometric approach: Vibration, buckling, and divergence analyses. Computer Methods in Applied Mechanics and Engineering. 2020;359:112668.

[44] Shafei E, Faroughi S, Rabczuk T. Isogeometric HSDT approach for dynamic stability analysis of general anisotropic composite plates. Composite Structures. 2019;220:926-39.

[45] Safaei B. The effect of embedding a porous core on the free vibration behavior of laminated composite plates. Steel and Composite Structures. 2020;35:659-70.

[46] Marchetti F, Ege K, Leclère Q, Roozen N. On the structural dynamics of laminated composite plates and sandwich structures; a new perspective on damping identification. Journal of Sound and Vibration. 2020:115256.

[47] Sinha L, Mishra S, Nayak A, Sahu S. Free vibration characteristics of laminated composite stiffened plates: Experimental and numerical investigation. Composite Structures. 2020;233:111557.

[48] Topal U, Dede T, Öztürk HT. Stacking sequence optimization for maximum fundamental frequency of simply supported antisymmetric laminated composite plates using teaching–learning-based optimization. KSCE Journal of Civil Engineering. 2017;21:2281-8.

[49] Narwariya M, Choudhury A, Sharma AK. Parametric study on Harmonic Analysis of anti-symmetric laminated composite Plate. Materials Today: Proceedings. 2018;5:20232-8.

[50] Javed S, Viswanathan K, Izyan MN, Aziz Z, Lee J. Free vibration of cross-ply laminated plates based on higher-order shear deformation theory. Steel and Composite Structures. 2018;26:473-84.

[51] Zhang Z, Li Y, Wu H, Chen D, Yang J, Wu H, et al. Viscoelastic bistable behaviour of antisymmetric laminated composite shells with time-temperature dependent properties. Thin-walled Structures. 2018;122:403-15.

[52] Shukla V, Vishwakarma P, Singh J. Buckling Analysis of Symmetric and Antisymmetric Laminated Plates with Meshfree Approach. Materials Today: Proceedings. 2019;18:4143-50.

[53] Sahla M, Saidi H, Draiche K, Bousahla AA, Bourada F, Tounsi A. Free vibration analysis of angle-ply laminated composite and soft core sandwich plates. Steel and Composite Structures. 2019;33:663.

[54] Belbachir N, Draich K, Bousahla AA, Bourada M, Tounsi A, Mohammadimehr M. Bending analysis of anti-symmetric cross-ply laminated plates under nonlinear thermal and mechanical loadings. Steel and Composite Structures. 2019;33:81-92.

[55] Belbachir N, Bourada M, Draiche K, Tounsi A, Bourada F, Bousahla AA, et al. Thermal flexural analysis of anti-symmetric cross-ply laminated plates using a four variable refined theory. Smart Structures and Systems. 2020;25:409-22.

[56] Chai H, Li Y, Zhang Z, Sun M, Wu H, Jiang S. Systematic analysis of bistable anti-symmetric composite cylindrical shells and variable stiffness composite structures in hygrothermal environment. The International Journal of Advanced Manufacturing Technology. 2020:1-17.

[57] Zhang W, Ma W, Zhang Y, Liu Y. Double excitation multi-stability and multi-pulse chaotic vibrations of a bistable asymmetric laminated composite square panels under foundation force. Chaos: An Interdisciplinary Journal of Nonlinear Science. 2020;30:083105.

[58] Chattibi F, Benrahou KH, Benachour A, Nedri K, Tounsi A. Thermomechanical effects on the bending of antisymmetric cross-ply composite plates using a four variable sinusoidal theory. Steel Compos Struct. 2015;19:93-110.

[59] Hu J, Lin S, Dai F. Pattern reconfigurable antenna based on morphing bistable composite laminates. IEEE Transactions on Antennas and Propagation. 2017;65:2196-207.

[60] Wang Y, Zhupanska OI. Modeling of thermal response and ablation in laminated glass fiber reinforced polymer matrix composites due to lightning strike. Applied Mathematical Modelling. 2018;53:118-31.

[61] Chillara V, Dapino MJ. Review of morphing laminated composites. Applied Mechanics Reviews. 2020;72.

[62] Mantzaroudis V, Stamatelos D. An approximate closed-form buckling solution for the local skin buckling of stiffened plates with omega stringers: The case of antisymmetric cross-ply and angle-ply laminations. Structures: Elsevier; 2020. p. 1196-209.

[63] Lopresto V, Antonio L, Serge A. Dynamic response and failure of composite materials and structures: Woodhead Publishing, 2017.

[64] Wang X. Differential Quadrature and Differential Quadrature Based Element Methods. Elsevier; 2015.

[65] Vescovini R, Dozio L, d'Ottavio M, Polit O. On the application of the Ritz method to free vibration and buckling analysis of highly anisotropic plates. Composite Structures. 2018;192:460-74.

Appendix A

$$\begin{Bmatrix} \varepsilon_{xx}^{(0)} \\ \varepsilon_{yy}^{(0)} \\ \gamma_{xy}^{(0)} \end{Bmatrix} = \begin{Bmatrix} \frac{\partial u_0}{\partial x} + \frac{1}{2}\left(\frac{\partial w_0}{\partial x}\right)^2 \\ \frac{\partial v_0}{\partial y} + \frac{1}{2}\left(\frac{\partial w_0}{\partial y}\right)^2 \\ \frac{\partial u_0}{\partial y} + \frac{\partial v_0}{\partial x} + \frac{\partial w_0}{\partial x}\frac{\partial w_0}{\partial y} \end{Bmatrix} \tag{A.1}$$

$$\begin{Bmatrix} \varepsilon_{xx}^{(3)} \\ \varepsilon_{yy}^{(3)} \\ \gamma_{xy}^{(3)} \end{Bmatrix} = -c_1 \begin{Bmatrix} \frac{\partial \varphi_x}{\partial x} + \frac{\partial^2 w_0}{\partial x^2} \\ \frac{\partial \varphi_y}{\partial y} + \frac{\partial^2 w_0}{\partial y^2} \\ \frac{\partial \varphi_x}{\partial y} + \frac{\partial \varphi_y}{\partial x} + 2\frac{\partial^2 w_0}{\partial x \partial y} \end{Bmatrix} \tag{A.2}$$

$$\begin{Bmatrix} \varepsilon_{xx}^{(1)} \\ \varepsilon_{yy}^{(1)} \\ \gamma_{xy}^{(1)} \end{Bmatrix} = \begin{Bmatrix} \frac{\partial \varphi_x}{\partial x} \\ \frac{\partial \varphi_y}{\partial y} \\ \frac{\partial \varphi_x}{\partial y} + \frac{\partial \varphi_y}{\partial x} \end{Bmatrix} \tag{A.3}$$

$$\begin{Bmatrix} \gamma_{yz}^{(0)} \\ \gamma_{xz}^{(0)} \end{Bmatrix} = \begin{Bmatrix} \varphi_y + \frac{\partial w_0}{\partial y} \\ \varphi_x + \frac{\partial w_0}{\partial x} \end{Bmatrix} \tag{A.4}$$

$$\begin{Bmatrix} \gamma_{yz}^{(2)} \\ \gamma_{xz}^{(2)} \end{Bmatrix} = -c_2 \begin{Bmatrix} \varphi_y + \frac{\partial w_0}{\partial y} \\ \varphi_x + \frac{\partial w_0}{\partial x} \end{Bmatrix} \tag{A.5}$$

Appendix B

$$\bar{Q}_{11} = Q_{11}cos^4\theta + 2(Q_{12} + 2Q_{66})sin^2\theta cos^2\theta + Q_{22}sin^4\theta \tag{B.1}$$

$$\bar{Q}_{12} = (Q_{11} + Q_{22} - 4Q_{66})sin^2\theta cos^2\theta + Q_{12}(cos^4\theta + sin^4\theta) \tag{B.2}$$

$$\bar{Q}_{22} = Q_{11}sin^4\theta + 2(Q_{12} + 2Q_{66})sin^2\theta cos^2\theta + Q_{22}cos^4\theta \tag{B.3}$$

$$\bar{Q}_{16} = (Q_{11} - Q_{12} - 2Q_{66})sin\theta cos^3\theta + (Q_{12} - Q_{22} + 2Q_{66})cos\theta sin^3\theta \tag{B.4}$$

$$\bar{Q}_{26} = (Q_{11} - Q_{12} - 2Q_{66})cos\theta sin^3\theta + (Q_{12} - Q_{22} + 2Q_{66})sin\theta cos^3\theta \tag{B.5}$$

$$\bar{Q}_{66} = (Q_{11} + Q_{22} - 2Q_{12} - 2Q_{66})sin^2\theta cos^2\theta + Q_{66}(cos^4\theta + sin^4\theta) \tag{B.6}$$

$$\bar{Q}_{44} = Q_{44}cos^2\theta + Q_{55}sin^2\theta \tag{B.7}$$

$$\bar{Q}_{45} = (Q_{55} - Q_{44})sin\theta cos\theta \tag{B.8}$$

$$\bar{Q}_{55} = Q_{55}cos^2\theta + Q_{44}sin^2\theta \tag{B.9}$$

$$\alpha_{xx} = \alpha_1 cos^2\theta + \alpha_2 sin^2\theta \tag{B.10}$$

$$\alpha_{yy} = \alpha_1 sin^2\theta + \alpha_2 cos^2\theta \tag{B.11}$$

$$\alpha_{xy} = (\alpha_1 - \alpha_2)sin\theta cos\theta \tag{B.12}$$

Appendix C

$$\begin{Bmatrix} N_{xx} \\ N_{yy} \\ N_{xy} \end{Bmatrix} = \begin{bmatrix} A_{11} & A_{12} & A_{16} \\ A_{12} & A_{22} & A_{26} \\ A_{16} & A_{26} & A_{66} \end{bmatrix} \begin{Bmatrix} \varepsilon_{xx}^{(0)} \\ \varepsilon_{yy}^{(0)} \\ \gamma_{xy}^{(0)} \end{Bmatrix} + \begin{bmatrix} B_{11} & B_{12} & B_{16} \\ B_{12} & B_{22} & B_{26} \\ B_{16} & B_{26} & B_{66} \end{bmatrix} \begin{Bmatrix} \varepsilon_{xx}^{(1)} \\ \varepsilon_{yy}^{(1)} \\ \gamma_{xy}^{(1)} \end{Bmatrix} + \begin{bmatrix} E_{11} & E_{12} & E_{16} \\ E_{12} & E_{22} & E_{26} \\ E_{16} & E_{26} & E_{66} \end{bmatrix} \begin{Bmatrix} \varepsilon_{xx}^{(3)} \\ \varepsilon_{yy}^{(3)} \\ \gamma_{xy}^{(3)} \end{Bmatrix} \tag{C.1}$$

$$\begin{Bmatrix} M_{xx} \\ M_{yy} \\ M_{xy} \end{Bmatrix} = \begin{bmatrix} B_{11} & B_{12} & B_{16} \\ B_{12} & B_{22} & B_{26} \\ B_{16} & B_{26} & B_{66} \end{bmatrix} \begin{Bmatrix} \varepsilon_{xx}^{(0)} \\ \varepsilon_{yy}^{(0)} \\ \gamma_{xy}^{(0)} \end{Bmatrix} + \begin{bmatrix} D_{11} & D_{12} & D_{16} \\ D_{12} & D_{22} & D_{26} \\ D_{16} & D_{26} & D_{66} \end{bmatrix} \begin{Bmatrix} \varepsilon_{xx}^{(1)} \\ \varepsilon_{yy}^{(1)} \\ \gamma_{xy}^{(1)} \end{Bmatrix} + \begin{bmatrix} F_{11} & F_{12} & F_{16} \\ F_{12} & F_{22} & F_{26} \\ F_{16} & F_{26} & F_{66} \end{bmatrix} \begin{Bmatrix} \varepsilon_{xx}^{(3)} \\ \varepsilon_{yy}^{(3)} \\ \gamma_{xy}^{(3)} \end{Bmatrix} \tag{C.2}$$

$$\begin{Bmatrix} P_{xx} \\ P_{yy} \\ P_{xy} \end{Bmatrix} = \begin{bmatrix} E_{11} & E_{12} & E_{16} \\ E_{12} & E_{22} & E_{26} \\ E_{16} & E_{26} & E_{66} \end{bmatrix} \begin{Bmatrix} \varepsilon_{xx}^{(0)} \\ \varepsilon_{yy}^{(0)} \\ \gamma_{xy}^{(0)} \end{Bmatrix} + \begin{bmatrix} F_{11} & F_{12} & F_{16} \\ F_{12} & F_{22} & F_{26} \\ F_{16} & F_{26} & F_{66} \end{bmatrix} \begin{Bmatrix} \varepsilon_{xx}^{(1)} \\ \varepsilon_{yy}^{(1)} \\ \gamma_{xy}^{(1)} \end{Bmatrix} + \begin{bmatrix} H_{11} & H_{12} & H_{16} \\ H_{12} & H_{22} & H_{26} \\ H_{16} & H_{26} & H_{66} \end{bmatrix} \begin{Bmatrix} \varepsilon_{xx}^{(3)} \\ \varepsilon_{yy}^{(3)} \\ \gamma_{xy}^{(3)} \end{Bmatrix} \tag{C.3}$$

$$\begin{Bmatrix} Q_y \\ Q_x \end{Bmatrix} = \begin{bmatrix} A_{44} & A_{45} \\ A_{45} & A_{55} \end{bmatrix} \begin{Bmatrix} \gamma_{yz}^{(0)} \\ \gamma_{xz}^{(0)} \end{Bmatrix} + \begin{bmatrix} D_{44} & D_{45} \\ D_{45} & D_{55} \end{bmatrix} \begin{Bmatrix} \gamma_{yz}^{(2)} \\ \gamma_{xz}^{(2)} \end{Bmatrix} \tag{C.4}$$

$$\begin{Bmatrix} R_y \\ R_x \end{Bmatrix} = \begin{bmatrix} D_{44} & D_{45} \\ D_{45} & D_{55} \end{bmatrix} \begin{Bmatrix} \gamma_{yz}^{(0)} \\ \gamma_{xz}^{(0)} \end{Bmatrix} + \begin{bmatrix} F_{44} & F_{45} \\ F_{45} & F_{55} \end{bmatrix} \begin{Bmatrix} \gamma_{yz}^{(2)} \\ \gamma_{xz}^{(2)} \end{Bmatrix} \tag{C.5}$$